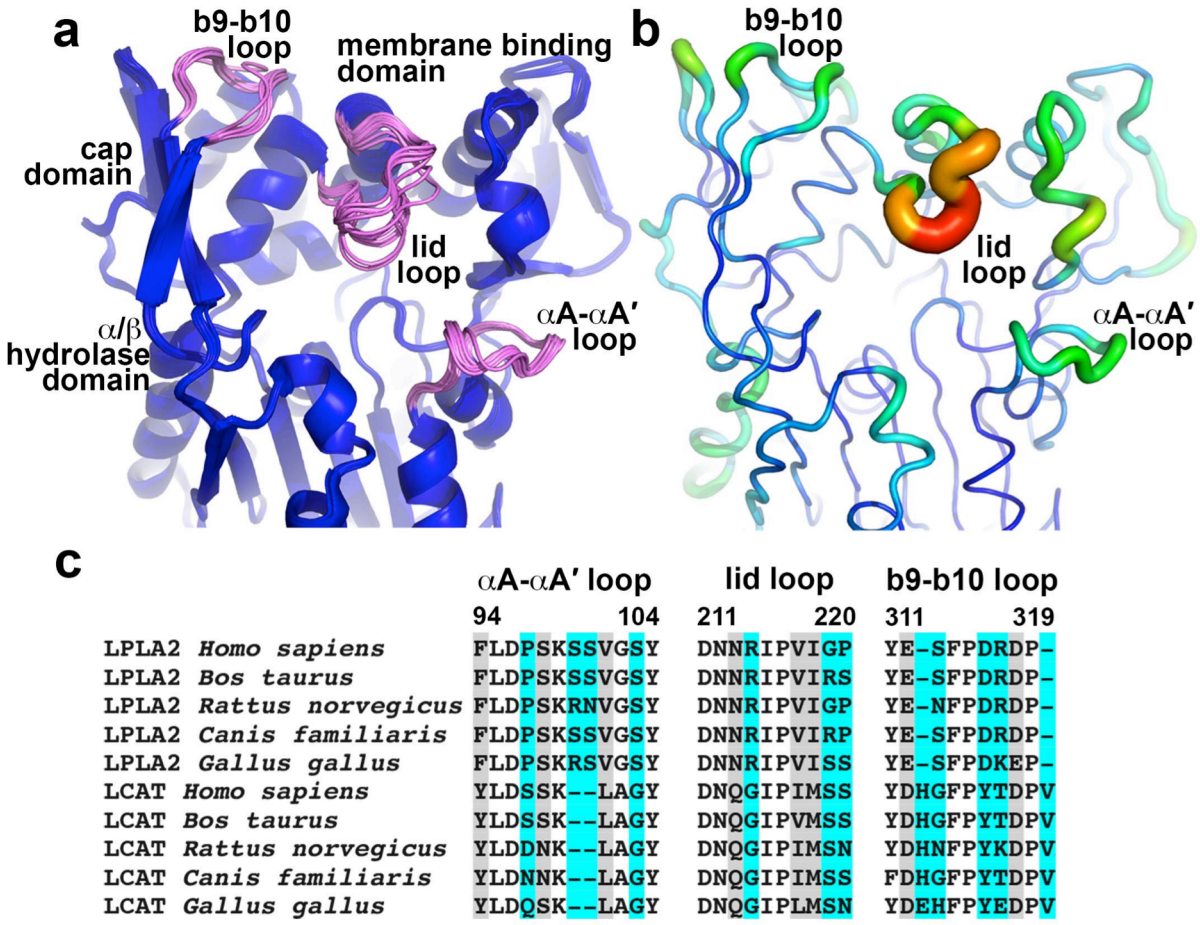

Figure 43. Conformational and sequence variability around track B. **(a)** Structural alignment of 16 unique LPLA2 chains from all of the unique LPLA2 crystal forms (Tables 2-4). Loops with highest RMSD scores (b9-b10 loop and lid loop of cap domain, and αA-αA´ of catalytic core) are shown in pink. **(b)** Temperature factor distribution is consistent with the conformational variability in panel A. Chain A of the apo LPLA2 structure with B-factors indicated by color (blue to red, 13 to 44 $Å^2$) and by width of the Cα trace. **(c)** Sequence alignment of the most flexible LPLA2 loops from different species with those of LCAT from the same species. Cyan and grey highlights indicate positions that are variable and highly conserved between LPLA2 and LCAT subfamilies, respectively. No highlight indicates invariance.

4.5 Membrane Association of LPLA2.

At lysosomal pH (~4.5), LPLA2 has an overall basic electrostatic surface that would complement the acidic inner leaflet of the lysosomal membrane (Fig. 44a). Examination of the structure also reveals a conserved, conspicuously solvent-exposed hydrophobic patch on the membrane binding domain that includes Tyr30, Leu31, Leu50, and Val52 (conserved as Trp48, Met49, Leu68 and Leu70 in LCAT) (Fig. 44a and b). Mutation of these residues to serine had no significant effect on T_m (data not shown) or on hydrolysis of the soluble substrate pNPB (Fig. 42a), indicating that all mutants were properly folded. However, all were significantly impaired in acyl transfer (Fig. 42b) and liposome binding (Fig. 42c). Control surface mutations (e.g. E47Q, V217S, K222A, R260/263A, L336A and K383A) had little or no significant effect in these assays. Taken together, these data confirm the existence of a lipid bilayer-binding site in the membrane binding domain.

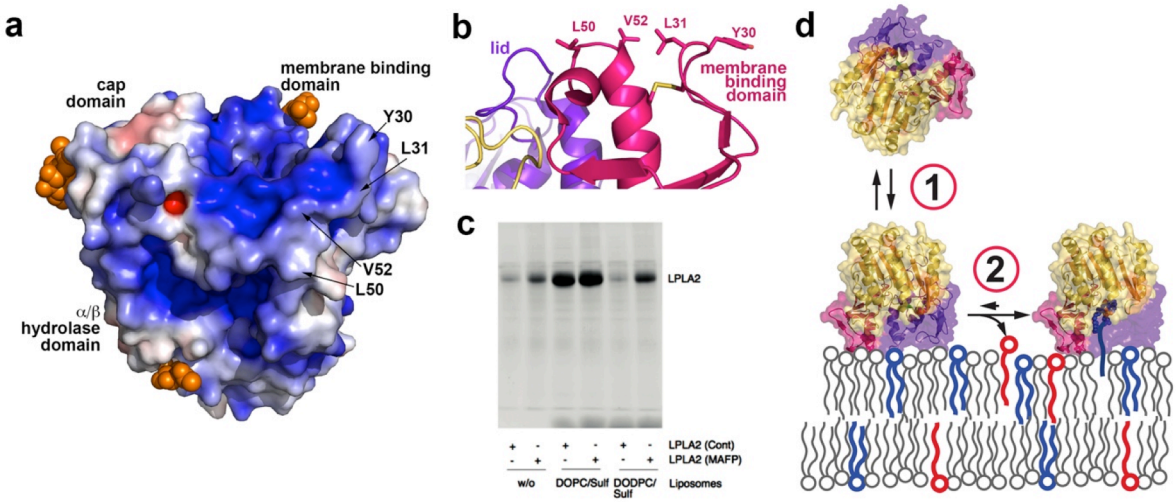

Figure 44. LPLA2 membrane association. **(a)** Electrostatic surface potential (± 5 kT/e) of LPLA2 at pH 5. Glycosylation sites (orange spheres) would not sterically interfere with the interaction between the membrane binding surface and lipid bilayers. **(b)** Proposed membrane binding surface of LPLA2. **(c)** LPLA2 requires either MAFP modification or substrate liposomes (DOPC-sulf) to stably associate with liposomes in pull down assays. Data shown is representative of four independent experiments. Experiment was performed by A. Abe. **(d)** Membrane association model. First, transient binding driven by complimentary electrostatic charge and the hydrophobic patch on the membrane binding domain. Second, formation of covalent acyl intermediate tethers LPLA2 at the membrane.

Unexpectedly, the S165A mutation was completely deficient in membrane binding (Fig. 42) despite being indistinguishable from wild-type LPLA2 in T_m (data not shown) and in overall atomic structure (Table 5, data not shown). This result implies that stable membrane association by LPLA2 in pull down assays requires catalytic turnover. If so, then LPLA2 reacted with IDFP and MAFP should also stably associate with liposomes. The amount of the inhibitor-bound LPLA2 co-sedimenting with DOPC-sulfatide liposomes was proportional to the length of the aliphatic arm of the phosphonate inhibitor with LPLA2·IDFP retaining 50% and LPLA2·MAFP 100% of apo LPLA2 binding (Fig. 42c). Thus, formation of an acyl intermediate seems to be required for stable LPLA2 membrane association, and if the liposomes do not contain a substrate for LPLA2, stable binding should not be observed. In support of this theory, LPLA2 did not associate with 1,2-*O*-dioctadecenyl-*sn*-glycero-3-phosphocholine (DODPC)-sulfatide liposomes, which are not substrates for LPLA2, but LPLA2·MAFP could (Fig. 44c). Therefore, LPLA2 membrane association occurs in at least two steps. First, LPLA2 transiently interacts with the inner leaflet of the lysosomal membrane by favorable electrostatic interactions (Abe & Shayman, 2009) and hydrophobic contacts mediated

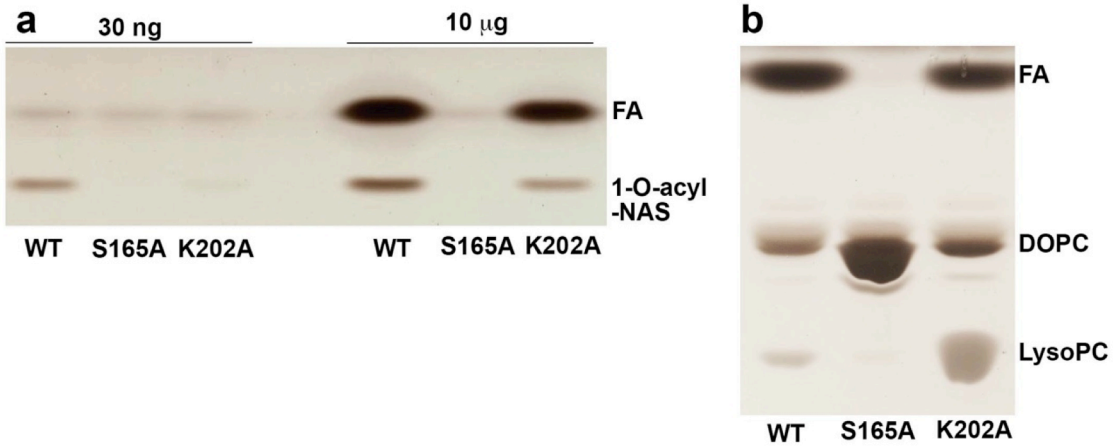

Figure 45. The LPLA2-K202A mutation reduces, but does not eliminate LPLA2 catalytic activity. **(a)** Transacylase assay using 3:10:1 molar ratio of NAS-DOPC-sulfatide liposomes. Reaction products relative to the negative control (S165A) are only observed at high enzyme concentrations. FA, fatty acid. **(b)** Esterase assay using (10:1) DOPC-sulfatide liposomes using 10 μg protein. Wild-type (WT) LPLA2 is more efficient at hydrolyzing both DOPC as well as the reaction product lysophosphatidic acid (LysoPC). K202A esterase activity is reduced judged by the amount of DOPC and LysoPC remaining after 30 min as well as by the amount of FA produced. Activity assays were performed by V. Hinkovska-Galcheva.

by its membrane binding domain. Next, the acyl intermediate formed during the catalytic cycle tethers LPLA2 to the membrane surface (Fig. 43d). Corroborating this mechanism, the K202A mutation greatly decreases the rate of DOPC deacylation (Fig. 45) without impacting membrane binding (Fig. 42c). It follows that after completion of the catalytic cycle LPLA2 would dissociate from the membrane. Similar behavior has been documented previously for LCAT. Product release triggers LCAT dissociation from HDL particles after each catalytic cycle (Adimoolam *et al.*, 1998).

4.6 LCAT Structure Determination.

Compared to LPLA2, LCAT has N- and C-terminal extensions that are not predicted to have secondary structure (Fig. 3). The LCAT residues 2-5 are however known to be important for LCAT activity, possibly by mediating contacts with ApoA-I in HDL particles (Vickaryous *et al.*, 2003). A glycosylated N-and C-terminally truncated variant of human LCAT ($LCAT_{21-397}$) had similar activity on soluble substrate pNPB and T_m as full length LCAT (Fig. 22). These data suggest that the N- and C-terminal extensions do not contribute to the core fold or active site of the enzyme. A homology model corresponding to the catalytic, membrane binding, and cap domains of LCAT was thus built based on the structure of LPLA2, which was subsequently used to successfully phase the 8.7 Å crystal structure of $LCAT_{21-397}$ (Table 6 and Fig. 46). The LCAT electron density maps reveal unbiased evidence for glycosylation at Asn84, Asn 272 and Asn 384, and all structural elements of the LCAT homology model fit well within the density envelope. Residues of LCAT analogous to those in the hydrophobic membrane binding patch in LPLA2 form a strong intermolecular crystal contact, wherein the Trp48 side chain of one chain binds deep into track B of another (Fig. 46c). This structure, albeit of low resolution, proves that the tertiary structure of LCAT is quite similar to that of LPLA2 and likely has the same functional surfaces, permitting the extension of results from higher resolution and functional studies of LPLA2 to LCAT, as well as a preliminary analysis of how these enzymes dictate selectivity for their acyl acceptor substrates.

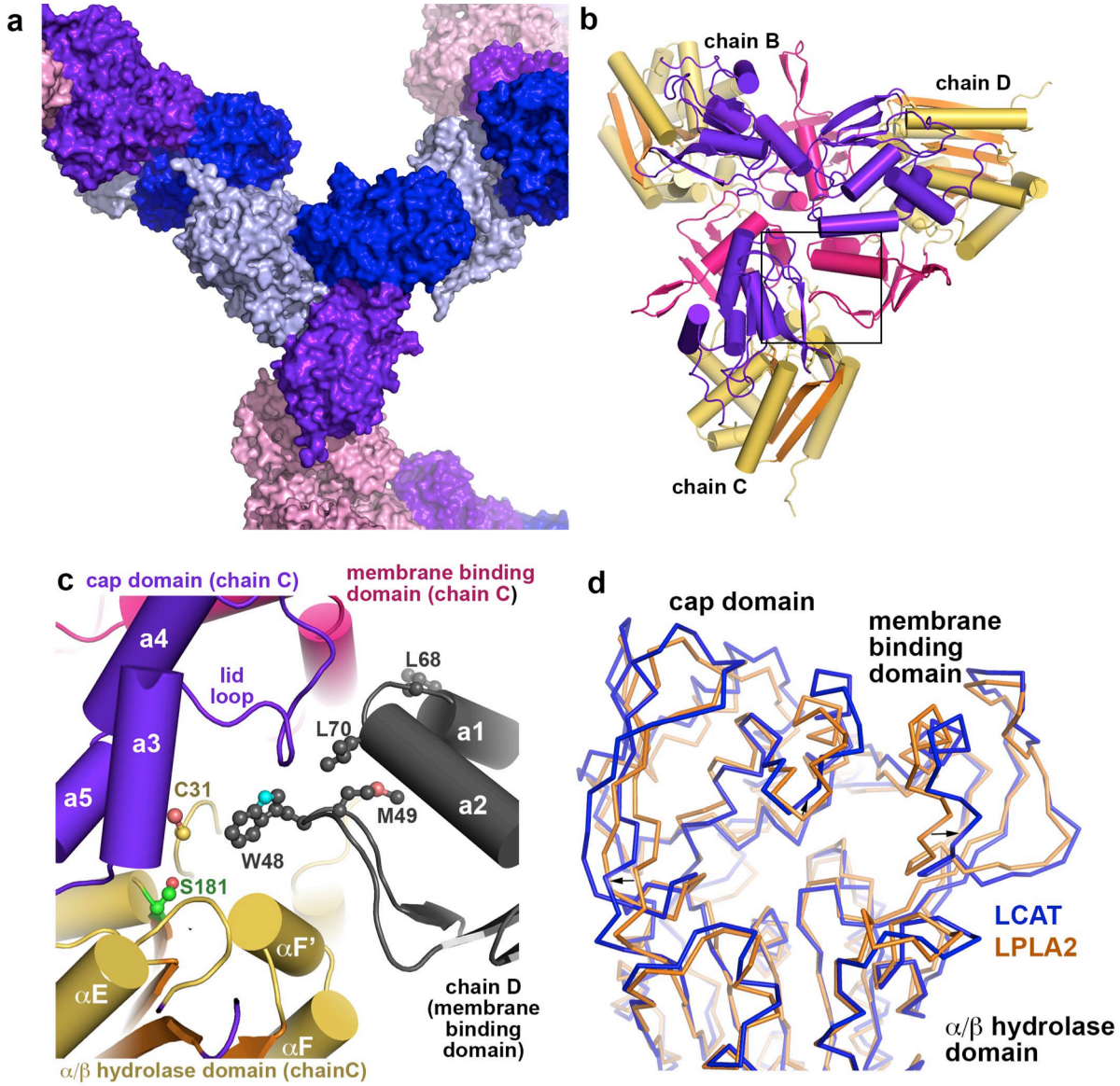

Figure 46. Structure of LCAT. **(a)** Surface representation showing lattice contacts in LCAT crystals, which contain 88% solvent (including sugar modifications estimated at 20 kDa (Schindler et al., 1995)). Each unique monomer is colored separately, and the four subunits form two homotrimers in the lattice, one non-crystallographic (chains B, C and D) and one crystallographic (chain A). **(b)** Non-crystallographic trimer formed by chains B, C, and D (there is however no evidence for oligomerization of LCAT in solution as assessed by size exclusion chromatography, data not shown). Domains are colored as for LPLA2 in Fig. 37. **(c)** Crystal contacts exploit the predicted membrane binding patch of LCAT, which packs into track B of each three-fold symmetry related subunit. **(d)** Structural variance in the membrane binding and cap domains of LPLA2 (gold Cα trace) and LCAT (blue Cα trace). The catalytic domains of LCAT and LPLA2 were aligned. Structural elements of LCAT that bracket the active site (arrows) seem to expand outwards by up to 4 Å. relative to LPLA2.

4.7 Molecular Basis for Acceptor Selectivity.

LPLA2 favors lipophilic alcohol acceptors, whereas the physiological acceptor of LCAT is cholesterol. Secondary alcohols such as cholesterol are not favored as acyl acceptors in LPLA2, and aliphatic alcohols are less efficient LCAT acceptors than sterols (Abe, Hiraoka, & Shayman, 2007b; Kitabatake *et al.*, 1979). Therefore, distinct features of the LPLA2/LCAT active sites must dictate substrate preference. One candidate based on sequence conservation and its topological position next to track B is the lid loop (Fig. 43c). The presence of a substantially larger and charged residue in LPLA2 (Arg214) relative to LCAT (Gly230) may discourage the binding of bulkier acyl acceptors such as secondary alcohols and sterols in track B. Indeed, structural alignment of LPLA2 and LCAT based on their α/β hydrolase domains suggests that multiple structural elements around the active site are expanded in LCAT relative to LPLA2, as if to increase the volume of the active site cleft (Fig. 46d). To test the role of the lid loop as a selectivity determinant, the LPLA2-N213Q/R214G mutant was assayed for cholesterol acyltransferase activity. Unfortunately, although this mutant had wild-type activity against soluble and lipid substrates (Fig. 42a,b), cholesterol ester formation was not observed under the acidic conditions required for LPLA2 activity (data not shown).

Models of NAS and cholesterol bound to LPLA2 and LCAT, respectively, are shown in Fig. 47, and support the idea that the lid loop could be a key selectivity determinant. The positioning of each molecule in the active site was constrained by the requirement for their nucleophilic hydroxyl groups to be close to the catalytic triad histidine as well as to Cys31 (analogous to Asp13 in LPLA2), a residue known to be important for cholesterol binding and activity regulation (Jauhiainen *et al.*, 1988). Indeed, mutations at LCAT-Cys31, which serve to enhance LCAT activity, are being patented for the treatment of atherosclerosis and coronary heart disease (Boone *et al.*, 2012).

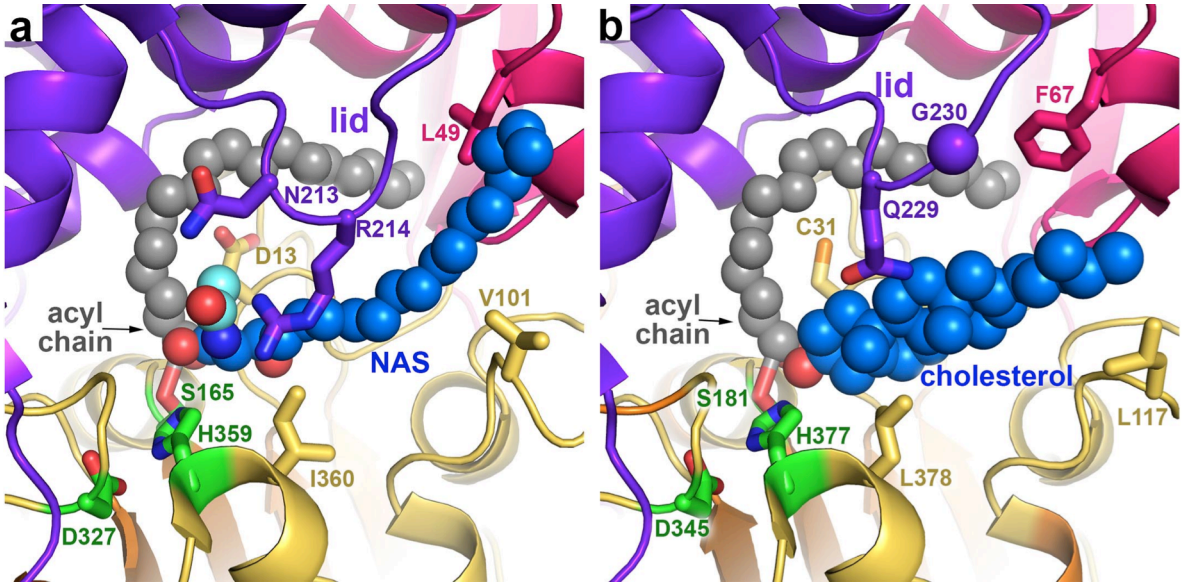

Figure 47. Models of acyl group acceptors in complex with LPLA2 and LCAT. **(a)** NAS in complex with LPLA2. Arg214 in the lid loop constrains the entrance to the active site near the catalytic triad, which as a result may favor the binding of narrower acceptor substrates. The ceramide side chain (cyan carbons) cannot be long given the packing environment. **(b)** Cholesterol in complex with LCAT. The presence of Gly230 (conserved as Arg214 in LPLA2) opens up track B such that it could accommodate bulkier acyl acceptors. In each panel, side chains of residues in track B that are different between LPLA2 and LCAT are drawn as sticks.

4.8 LCAT Somatic Mutations.

FLD and FED patients are both diagnosed with corneal opacification, whereas clinical manifestations of FLD also include anemia, proteinuria, and renal failure. More than 80 mutations in the human LCAT gene have been described to date (www.lcat.it). Whereas insertions, deletions and early terminations lead to complete loss of function, missense mutations harbor unique structural and functional information about LCAT and, consequently, LPLA2. The crystal structures of LPLA2 and LCAT were thus used to identify the molecular defects underlying 53 missense LCAT mutations (Table 8). The phenotype of specific mutations was correlated with the clinical phenotype (FLD or FED, although assigning phenotype is often complicated by late onset of symptoms, compound heterozygosity, or environmental factors) and relative levels of α- and β-LCAT activities.

Table 8. Molecular basis for disease in known FED and FLD mutations

Mutation	Clinical phenotype	α LCAT activity	β LCAT activity	Ref.	Explanation
Structural Variants (suspected folding/processing defects)					
V28M	FLD (CH with A211T)	na	na	(Weber, Frohlich, Wang, Hegele, & Chan-Yan, 2007)	Disruption of packing in core of catalytic domain.
D77N	FLD (CH with T106A)	na	na	(Aranda et al., 2008)	Loss of salt bridge between Asp^{77} and Lys^{42}.
V90M	NC	na	na	(Cohen et al., 2004)	Disrupts packing between membrane-binding and cap domain.
S91P	FED (CH with A141T)	↓↓↓ (inv;rH)	↓↓↓ (inv;LDL)	(Calabresi et al., 2009; 2005)	Disrupts secondary structure of the b4-b5 hairpin in membrane binding domain.
A93T	FLD (HZ with R158C)	↓↓↓ (inv;rH)	↓↓↓ (inv;LDL)	(Funke et al., 1993; Hill, O, Wang, & Pritchard, 1993a; Qu, Fan, Blanco-Vaca, & Pownall, 1995)	Potentially disrupts salt bridge between Asp^{77} and Lys^{42}.
R99C	FED	↓↓↓ (inv;rH)	↓↓↓ (inv;LDL)	(Blanco-Vaca et al., 1997)	Loss of salt bridge with Glu^{35} and of stacking interaction with Phe^{57}.
T106A	FLD (CH with D77N)	na	na	(Aranda et al., 2008)	Loss of hydrophobic interactions with Val^{125} and Arg^{135}, and of hydrogen bond with Glu^{110}.
E110D	NCh	↓↓↓ (inv;rH;NC)	na	(Holleboom, Kuivenhoven, Peelman, et al., 2011a)	Possible structural defect. Loss of salt bridge with His^{122} and Arg^{135} (residues conserved in LPLA2).
Y111N	NCh	↓↓↓ (inv;rH;NC)	na	(Holleboom, Kuivenhoven, Peelman, et al., 2011a)	Disrupts packing interactions with αA-αA′ loop (Fig. 43).
R135Q	FED (CH with P10Q)	↓↓↓ (inv;rH)	↓↓↓ (inv;LDL)	(Kuivenhoven et al., 1996)	Loss of salt bridge with Glu^{110}.*
R135W	FLD (CH with Q347T and 416Ter)	↓↓↓ (inv;rH)	↓↓↓ (inv;LDL)	(Funke et al., 1993; Qu et al., 1995)	Loss of salt bridge with Glu^{110}. Possible altered solubility due to introduction of a solvent exposed hydrophobic residue.*
R140H	INT (CH with G71R)	↓↓↓ (inv;rH)	↓↓↓ (inv;LDL)	(Hörl et al., 2006)	Histidine likely incompatible with packing.*
R140C	FLD	↓↓↓ (inv;rH;NC)	na	(Steyrer et al., 1995)	Cysteine cannot fully reproduce arginine packing interactions.
A141T	FED (CH with S91P)	↓↓↓ (inv;rH)	wt (inv;LDL)	(Calabresi et al., 2005; 2009)	Destabilization of catalytic domain via introduction of a larger side chain. May perturb structure only locally such that it retains binding to LDL particles.
Y144C	FED (CH with T123I)	↓↓↓ (PL;DPL)	↓ (PL;CER)	(Contacos, Sullivan, Rye, Funke, & Assmann, 1996)	Creation of cavity due to shorter cysteine side chain.
R147W	FLD	↓↓↓ (inv;rH)	↓↓↓ (inv;LDL)	(Calabresi et al., 2005; 2009)	Loss of salt bridge to Asp^{145} and introduction of steric clashes between catalytic and membrane binding domains. *
Y156N	FLD (CH with Y83Ter)	↓↓ (inv;rH)	↓↓↓	(Klein et al., 1995; 1993)	Creation of cavity due to shorter asparagine side chain.*
G179R	FLD	↓↓↓	na	(X. L. Wang et al., 2011)	Introduction of steric clashes and charge via larger charged side chain.
G183S	FLD	↓↓↓	na	(J. McLean, 1992)	Mutation interferes with nucleophilic elbow folding and/or catalytic activity.*
L209P	FLD	na	na	(Funke et al., 1993;	Pro substitution perturbs secondary structure in

		(inv;NP)	(inv;NP)	Qu et al., 1995)	β4 strand.*
A211T	FLD (CH with V28M)	na	na	(Weber et al., 2007)	Destabilization by introduction of steric clashes.
R244C	FLD (CH with L32P)	na	na	(Charlton-Menys et al., 2007)	Loss of hydrogen bonds and packing interactions.
R244H	FED	0 (inv;rH)	wt (inv;LDL)	(Calabresi et al., 2009)	Loss of hydrogen bonds and packing interactions.
T274A	FED (FLD symptoms) (CH with Y83Ter)	↓↓↓ (PL;rH)	wt (PL;CER)	(Calabresi et al., 2005)	Glycosylation defect (alteration in NxT consensus). Likely structural defect.
T274I	FLD	↓↓↓ (inv;rH)	↓↓↓ (inv;LDL)	(Calabresi et al., 2005; 2009)	Glycosylation defect (alteration in NxT consensus). Likely structural defect.
M293R	FLD	na	na	(Roshan et al., 2011)	Disrupts packing between cap domain and b4-b5 hairpin of membrane binding domain.
M293I	FLD	↓↓↓ (inv;rH)	↓↓↓ (inv;CER)	(Gotoda et al., 1991; Klein et al., 1995)	Disrupts packing between cap domain and b4-b5 hairpin of membrane binding domain.
P307S	FLD (CH with T13M)	na	na	(Argyropoulos et al., 1998)	Loss of packing interactions.
V309M	FLD	↓↓↓ (inv;rH)	↓↓↓ (inv;LDL)	(Calabresi et al., 2009)	Introduction of steric clashes via larger side chain.
C313Y	FLD	na (inv;NP)	na (inv;NP)	(Holleboom, Kuivenhoven, van Olden, et al., 2011b)	Loss of disulfide bridge between β7 and αE in catalytic domain.
L314F	FED (CH with R323C)	↓↓ (inv;rH)	na	(Holleboom, Kuivenhoven, Peelman, et al., 2011a)	Introduction of steric clashes via larger side chain.
L372R	FLD	↓↓↓ (inv;rH)	↓↓↓ inv;LDL)	(Calabresi et al., 2009)	Introduction of steric clashes via larger side chain.
Catalytic Variants (interfere with substrate binding and/or catalysis)					
G30S	FLD	↓↓↓ (inv;rH)	na	(Rosset, Wang, Wolfe, Dolphin, & Hegele, 2001; X. P. Yang et al., 1997)	Disruption of oxyanion hole.
L32P	FLD	na	na	(Charlton-Menys et al., 2007)	Disruption of oxyanion hole; likely packing defect.
G33R	FLD (CH w/ 30 bp ins)	↓↓↓ (PL;rH)	↓↓↓ (PL;CER)	(Wiebusch et al., 1995)	Structural defect as well as occlusion of track B (phospholipid and cholesterol binding defect).
W75R	INT	na	na	(Charlton-Menys et al., 2007)	Introduction of charge into track A and possible membrane binding domain destabilization.
W75S	FED (CH with T123I)	↓↓↓ (inv;rH;NC)	na	(Holleboom, Kuivenhoven, Peelman, et al., 2011a)	Modulation of track A and possible membrane binding domain destabilization.
S181N	FLD (CH with a frame shift)	↓↓↓ (inv;rH)	↓↓↓ (inv;LDL)	(Calabresi et al., 2005; 2009; Frascà et al., 2004)	Loss of nucleophilic serine essential for catalysis.
K218N	FLD	↓↓↓ (inv;rH)	↓↓↓ (inv;LDL)	(Calabresi et al., 2005; 2009)	Loss of residue proposed to be involved in binding phospholipid head group (cf. LPLA2-Lys^{202}).
N228K	FLD	↓↓↓ (inv;rH)	↓↓↓ (inv;CER)	(Adimoolam et al., 1998; Gotoda et al., 1991; Klein et al., 1995)	Possible structural defect in lid loop and defects in substrate binding.
G230R	FLD	↓↓↓ (inv;rH;NC)	na	(H. E. Miettinen et al., 1998)	Possible defects in substrate binding (cf. LPLA2-Arg^{214})

M252K	FLD	↓↓↓ (PL;rH)	na	(Skretting, Blomhoff, Solheim, & Prydz, 1992)	Introduction of a charged residue into track A.
T321M	FLD	na (inv;NP)	na (inv;NP)	(Funke et al., 1993; Qu et al., 1995)	Introduction of steric clashes via larger side chain and disruption of loop bearing triad residue Asp^{345}.
G344S	FLD	na (inv;NP)	na (inv;NP)	(Moriyama et al., 1995)	Introduction of steric clashes via larger side chain.*
T347M	FED (CH with T123I)	↓↓↓ (inv;rH)	↓↓↓ (inv;LDL)	(Klein et al., 1995; 1992; Qu et al., 1995)	Mutates position likely involved in coordination of phospholipid head group (cf. LPLA2-Thr^{329}); inhibition of substrate binding.*
HDL and LDL binding defects					
V46E	FED	↓↓↓ (inv;rH)	↓ (inv;CER)	(Calabresi et al., 2005; Calabresi & Francheschini, 2010)	Destabilization likely via electrostatic repulsion with D73 and D77.
G71R	INT (CH with R140H)	↓↓↓ (inv;rH)	↓↓↓ (inv;LDL)	(Hörl et al., 2006)	Disruption of membrane binding interface.
T123I	FED	↓↓↓ (inv;rH)	wt (inv;LDL)	(Contacos et al., 1996; Funke et al., 1991; Hill, Wang, & Pritchard, 1993b; Klein et al., 1992; Qu et al., 1995)	Putative ApoA-I binding site.*
N131D	FED	↓↓↓ (inv;rH)	↓↓ (inv;LDL)	(Kuivenhoven et al., 1995)	Putative ApoA-I binding site.*
F382V	FLD (CH with T321M)	↓↓ (PL;rH;NP)	↓↓↓ (PL;CER; NP)	(Nanjee, 2003)	Putative ApoA-I binding site based on its position. Unclear why b-LCAT activity is also affected.
N391S	FED (CH with M252K)	↓↓↓ (inv;rH)	wt (inv;LDL)	(Rader et al., 1994; Vanloo et al., 2000)	Putative ApoA-I binding site.*
Ambiguous					
R158C	FLD (HZ with A93T)	↓↓ (inv;rH)	wt (inv;LDL)	(Hill et al., 1993a; Klein et al., 1995; Qu et al., 1995)	Possible loss of favorable electrostatic interactions with Glu^{154} and Glu^{155}, or loss of activity due to side chain oxidation.
R323C	FED (CH with L314F)	↓ (inv;rH)	na	(Holleboom, Kuivenhoven, Peelman, et al., 2011a)	Possible loss of activity due to side chain oxidation.

Rows of the table are shaded according to the domain assignment of each position (see Fig. 37): α/β hydrolase domain (yellow), membrane binding domain (light pink), or cap domain (light purple). CER, plasma cholesterol esterification rate (therefore both α and β LCAT activities); CH, compound heterozygous; DPL, assay on LDL/VLDL depleted plasma; HZ, homozygous, both mutation occur on a single allele; INT, intermediate phenotype; inv, expressed *in vitro*; LDL, assay on isolated ApoB-containing lipoproteins; na, not assayed; NC, no control for LCAT expression level; NCh, phenotype was not characterized; NP, undetectable or low protein levels**;** PL, assay using patient's plasma; rH, assay on recombinant HDL proteoliposomes; wt, activity comparable to wild type LCAT. ↓, ↓↓ and ↓↓↓ correspond to mild, medium and severe reduction in LCAT activity, respectively. α LCAT activity, activity on HDL particles; β LCAT activity, activity on ApoB containing lipoproteins.

*Similar explanations for these variants were proposed using models of the catalytic core built by threading algorithms (Peelman et al., 1998; 1999).

Many FLD mutations result in structural defects that likely impact the folding, processing, and/or structural stability of LCAT (Fig. 48a and b). These include defects in the core of the catalytic domain such as V28M, T106A, E110D, Y111N, R135Q/W, R140H/C, A141T, Y144C, Y156N, L209P, A211T, P307S, V309M, C313Y, L314F, and L372R, or of the cap domain such as R244H/C and T274A/I (the latter of which is also likely a glycosylation defect). FLD-causing mutations are located in the interface between the b4-b5 loop of the membrane binding domain and the cap domain (V90M, S91P, and M293R/I), supporting the idea that this belt-like interdomain contact critical for the overall fold of the enzyme. An inactivating R147W mutation is found between the membrane-binding and catalytic domains, likewise suggesting that the integrity of this interface is structurally important.

Other inactivating mutations perturb the catalytic machinery (Fig. 49a and b). The backbone amides of Cys31 and Leu182 form the oxyanion hole in LCAT, and mutation of residues in close proximity such as G30S, L32P, and G33R consequently all lead to the FLD phenotype in human patients. The G179R, S181N, and G183S mutations eliminate activity by perturbing the conformationally strained nucleophile elbow that contains the active site serine, as previously predicted (Peelman *et al.*, 1999).

Another class of mutations supports the assigned roles of tracks A and B and of residues coordinating the phospholipid head group (Fig. 49a and b). The G33R mutation, if it folds, would obstruct track B and block acyl acceptor binding. The W75R and M252K mutations would introduce positive charges into track A. T347M, which leads to almost complete loss of LCAT activity on HDL and LDL bound cholesterol when expressed *in vitro* (Qu *et al.*, 1995), is consistent with the catalytic defects exhibited by LPLA2-T329A. The LCAT K218N mutation, which results in full loss of activity (Calabresi *et al.*, 2009), is likewise consistent with catalytic defects exhibited by the LPLA2-K202A mutation (Fig. 49a and b). Mutations in the lid loop also generate the FLD phenotype (Gotoda *et al.*, 1991; H. E. Miettinen *et al.*, 1998). N228K and G230R (interestingly, reverting the latter position to its equivalent in LPLA2) greatly diminish the activity of LCAT, consistent with a role in binding substrates.

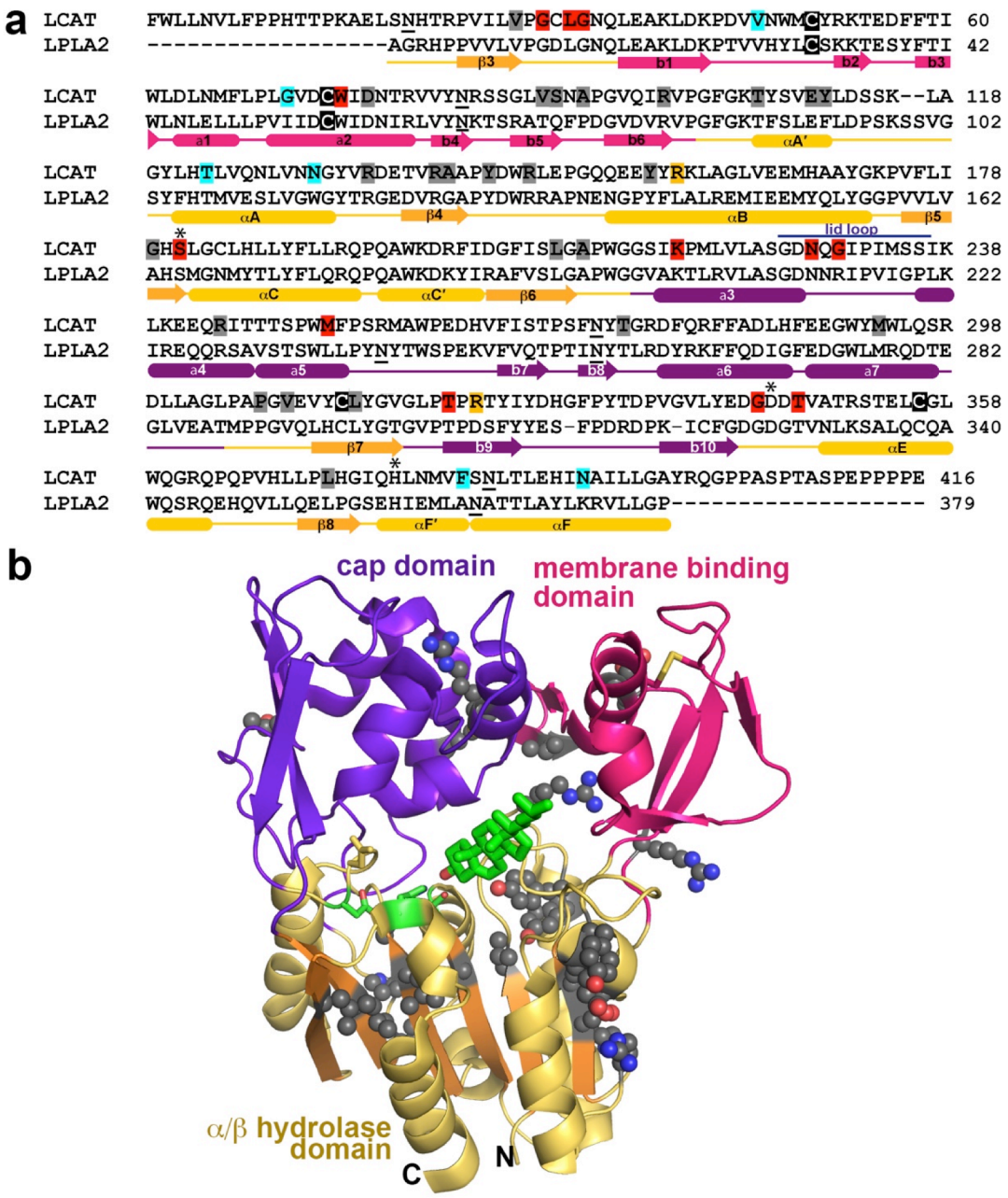

Figure 48. FLD and FED somatic mutations of LCAT. **(a)** Sequence alignment of mature human LPLA2 and LCAT. Positions that when mutated are predicted to have structural defects are highlighted gray, catalytic defects red, HDL binding defects cyan, and undetermined yellow. Cysteines engaged in disulfide bonds are highlighted black. N-linked glycosylation sites are underlined. Purple line indicates the lid loop of LPLA2. **(b)** Structural mutations (spheres with grey carbons) most likely cause defects in LCAT folding, stability, and/or sorting. Mutations affecting the LCAT active site (side chains shown as red spheres) cluster around the catalytic triad (green carbons) and predicted cholesterol (green stick model) binding site.

Of particular interest are mutations of residues on or near the surface of LCAT that do not have a clear explanation for loss of activity and/or have an FED phenotype (Fig. 49c and d). The V46E and G71R mutations are located in the membrane-binding domain, in close proximity to the proposed membrane-binding surface, and thus likely disrupt membrane association. The T123I, N131D, R135Q/W, F382V, and N391S mutations are located on a contiguous surface of the catalytic domain spanning helices αA´, αA, and αF (Fig. 49d). This region is also in close proximity to the N-terminal extension of LCAT, which is known to be important for activity on HDL(Vickaryous *et al.*, 2003). This region may therefore represent a macromolecular interaction site for HDL particles, as suggested by site-directed mutagenesis and antibody-binding experiments(Murray *et al.*, 2001; Vanloo *et al.*, 2000). However, only Asn^{131}, Phe^{382}, and Asn^{391} are not conserved in LPLA2, indicating that some of the residues in this region may simply be playing a structural role. The functional role of this surface and how ApoA-I binding at this site might lead to LCAT activation remains to be determined.

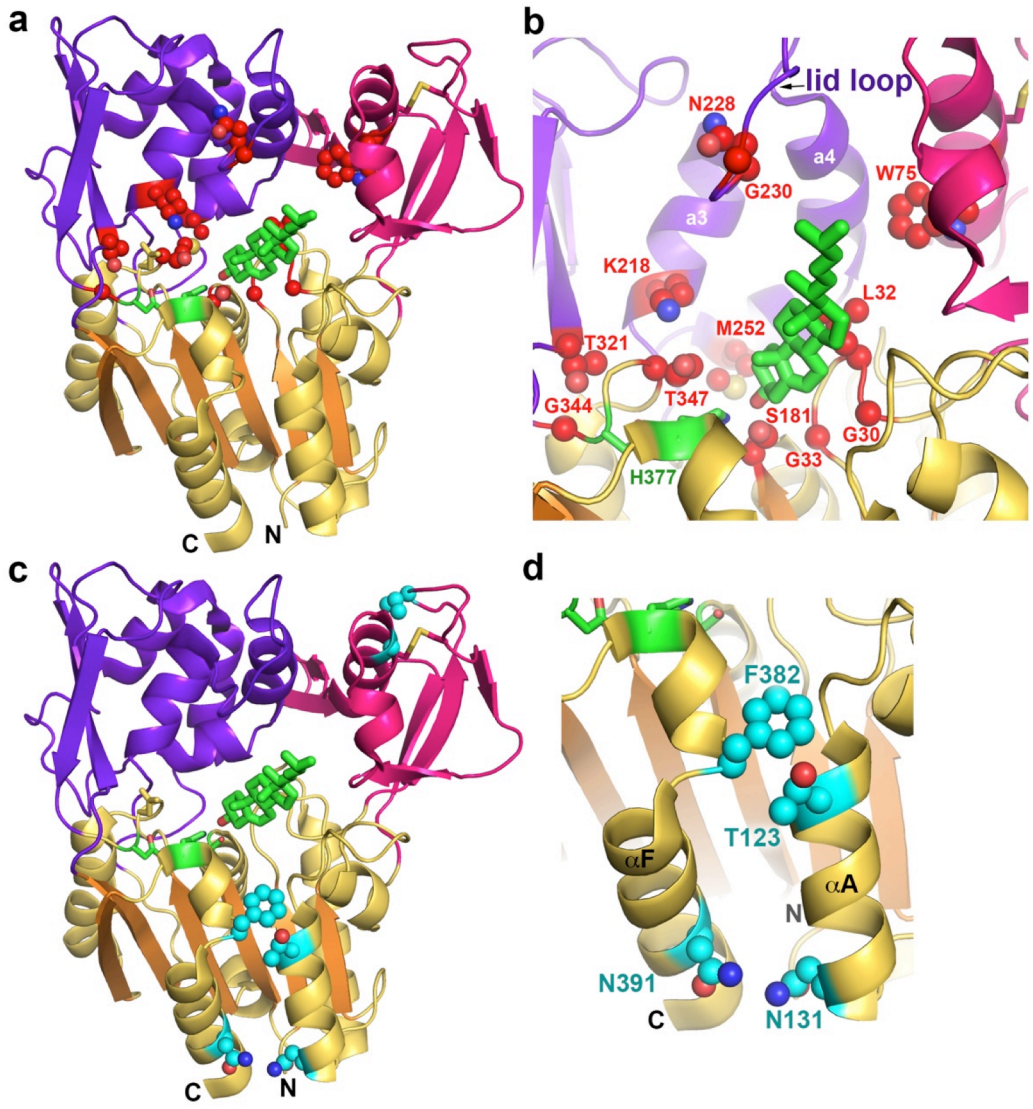

Figure 49. Overview of positions mutated in FLD and FED patients mapped onto the structure of LCAT. **(a)** Catalytic mutations (spheres with red carbons) most likely interfere with LCAT catalytic functions either by structural perturbation of catalytic residues or by inhibiting substrate binding. **(b)** Mutations affecting the LCAT active site (side chains shown as red spheres) cluster around the catalytic triad (green carbons) and predicted cholesterol (green stick model) binding site. **(c)** Mutations that likely interfere either with membrane or HDL binding (spheres with cyan carbons). Cholesterol (stick model with green carbons) is modeled in the active site for reference. **(d)** FED mutations (side chains shown as cyan spheres) tend to be found on the surface of the protein, the most prominent cluster being on the catalytic domain close to the N and C-termini of the enzyme.

Conclusions and future directions

We determined crystal structures of LPLA2 and LCAT, revealing the unique architecture of a small family of lipid metabolizing enzymes that play important roles in human physiology and disease. LCAT and LPLA2 have an α/β hydrolase and two additional domains with unique folds: the cap and membrane binding domain. Despite the fact that the cap domain has no homology to cap domains of triacylglycerol lipases, they share several topological features. When present, the cap domain in triacylglycerol lipases forms a part of the substrate-binding site for phospholipids. Similarly, in both LCAT and LPLA2, the cap domain helps form a hydrophobic track for the scissile acyl chain. Structural alignment of the type I bacterial lipases reveled that helixes a3 and a5 of LPLA2 and helixes α4 and α6 of lipases have an similar positioning relative to the α/β hydrolase domain and the active site. The presence of such structurally similar elements in very distantly related protein represents a remarkable example of divergent evolution, when the function (in this case – binding of hydrophobic acyl chains) dictates the conservation of certain structural elements.

Mobile lids of bacterial lipases, which regulate the substrate access into the active site, are typically inserted between helixes α4 and α6. The corresponding lid loop of LPLA2 seems to be flexible but unable to shield the active site in an analogous way. Despite solving multiple high-resolution structures of LPLA2, we have yet to see large-scale changes in this structural element. Thus, we suggested that, contrary to triacylglycerol lipases, LPLA2 does not exhibit interfacial activation. However, more straightforward experiments should be performed to answer this question, for example the investigation of dependence of the pNPB hydrolysis rate on the presence of detergents, micelles, or lipid bilayers. It has been reported previously that the rate of pNPB hydrolysis by LCAT increases in the presence of nonionic detergents, such as Triton X-100 or N,N-Bis[3-(D-gluconamido)propyl]cholamide (Bonelli & Jonas, 1993). It

would be interesting to learn if these detergents have similar effect on LPLA2, or if the presence of lipid bilayers could have a more profound effect.

In bacterial lipases that do undergo interfacial activation, opening of the lid exposes an extremely hydrophobic surface for binding to lipid surfaces. In lipases that do not undergo interfacial activation, such as *Bacillus subtilis* lipase, the hydrophobic membrane-binding interface is presented permanently (van Pouderoyen *et al.*, 2001). LPLA2 and LCAT both have a relatively modest exposure of hydrophobic residues at their predicted membrane-binding interface. However, these enzymes might employ different strategies for membrane binding. LCAT interacts with apoproteins on HDL and LDL particles (C. J. Fielding *et al.*, 1972), and interaction with ApoA-I dramatically increases LCAT catalytic activity, presumably through direct protein-protein interactions. On the other hand, LPLA2 activity is strongly dependent on pH, and is the highest at pH 4.5, a pH commonly found in lysosomes and in local inflammation events (Abe & Shayman, 1998). At such acidic pH, many groups are at least partially protonated, neutralizing negative charge on the protein surface. As lysosomal membranes are negatively charged due to the presence bis(monoacylglycero)phosphate (BMP), the electrostatic repulsion is weakened between LPLA2 and the membrane at low pH. Presumably, in such environment even weak hydrophobic interactions would be sufficient to bring LPLA2 to the membrane interface.

However, LPLA2 and, most probably, LCAT employ an additional unique method for membranes anchoring during a catalytic cycle. As we have shown in this study, catalytic activity or the formation of the catalytic intermediate is necessary for stable LPLA2 membrane association (Fig. 44). Thus we proposed a two-step mechanism for membrane binding. The first step includes the transient interaction between the small hydrophobic patch of LPLA2 and weak electrostatic interactions. The second step involved high affinity interactions between the acyl chains of a phospholipid substrate bound in the LPLA2 active site and the membrane. Our model is supported by previously published data showing LCAT dissociation from HDL particles after each catalytic cycle (Adimoolam *et al.*, 1998).

Despite the fact that our low resolution LCAT structure is supported the LPLA2-based homology model, we cannot exclude the possibility that LPLA2 and LCAT are

fundamentally different in terms of the interfacial activation. It is possible, that ApoA-I activation of LCAT results from some conformational change. Thus, a higher resolution structure of LCAT would be desirable to identify regions that might be responsible. In addition, full length LCAT has additional 20 amino acids on its N-terminus that are absent in LPLA2 or in the crystallized $LCAT_{21-397}$ construct. Deletion of those amino acids resulted in the loss of LCAT activity on either LDL or HDL particles (Vickaryous *et al.*, 2003). Although it is more likely that the hydrophobic N-terminus is involved in membrane interactions, it is possible that some unaccounted interaction takes place between the LCAT N-terminus and the protein core, exhibiting an effect on enzyme activity.

LCAT crystallization clearly has been a challenge for over the past 15 years, when first reports attempting to prepare crystallization quality materials have emerged (Chisholm *et al.*, 1999). As LPLA2, LCAT has four sites of N-linked glycosylation. In addition it also has O-linked glycosylation sites and unstructured regions at the extreme N-and C-terminus. Another difference from LPLA2 is LCAT's extreme sensitivity to the composition of the N-linked polysaccharides. As such, its expression levels were very low when we attempted to convert the normally complex glycosylation into the high-mannose type either by LCAT expression in HEK293S GnTi$^-$ cells or by inhibiting the α-mannosidase I activity in the HEK 293T cells by kifunensine. Luckily, such sensitivity does not apply if the polysaccharide addition is inhibited at the α-mannosidase II stage by another inhibitor swainsonine. Protein, expressed in HEK 293T cells in the presence of swainsonine could be a promising lead for the future LCAT crystallization trials.

In addition to the determination of a high resolution structure of LCAT, future goals also include better understanding the molecular rules for substrate selectivity and the roles of Asp^{13} and Cys^{31}, which, along with the studies presented here, could be used to design improved therapeutics to treat FED, FLD, and cholesterol-related disorders. In addition, we would like to understand how LCAT is activated by HDL and, in particular, by ApoA-I.

Appendix: GRK5 membrane binding and regulation by Ca^{2+}-CaM

A.1 Introduction

G protein-coupled receptor (GPCR) activation by extracellular signals leads to downstream signaling through heterotrimeric G proteins and second messenger-mediated activation of important intracellular effectors such as protein kinase A and C (PKA and PKC), phospholipase C, ion channels and others (Pitcher, Freedman, & Lefkowitz, 1998). GPCR signaling can be terminated on the receptor level by either homologous or heterologous desensitization (Ferguson, 2001). The latter mechanism is mediated by kinases with broad selectivity, such as PKA, and PKC. The first step of homologous desensitization is mediated solely by G protein-coupled receptor kinases (GRKs). They phosphorylate agonist-bound GPCRs on either the C-terminus (Fredericks, Pitcher, & Lefkowitz, 1996) or the third intracellular loop (Liggett *et al.*, 1992) creating the binding sites for β-arrestins, eventually leading to receptor internalization via endocytosis (Ferguson, 2001; Hanyaloglu & Zastrow, 2008).

A.1.1 The GRK subfamily

GRKs are a small subfamily within the family of AGC serine/threonine kinases, named after protein kinases A, G and C (Arencibia, Pastor-Flores, Bauer, Schulze, & Biondi, 2013). Unlike most other members of the subfamily, GRKs do not require phosphorylation of their activation loops to achieve a catalytically competent state. To date seven members of the GRK family have been identified (GRK1-7). They are grouped into three subfamilies based on their sequence similarity: the GRK1 subfamily (GRK1 and GRK7), the GRK2 subfamily (GRK2 and GRK3) and the GRK4 subfamily (GRK4-6). All GRKs have a conserved kinase domain, a regulatory RGS-homology (RH) domain and highly variable C-terminal extension. Located within the C-terminus

are many regulatory domains/elements, such as sites for PKC phosphorylation, autophosphorylation, and binding motifs for Gβγ subunits and Ca^{2+}-binding proteins. Also, in all GRKs, the C-terminus contains elements responsible for their membrane recruitment and/or localization (Fig. 50).

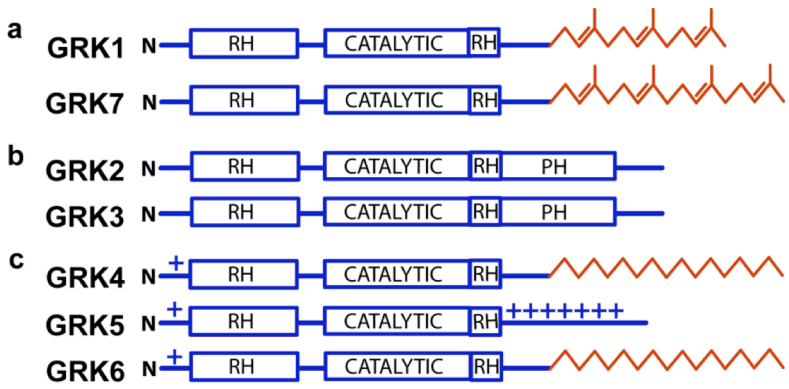

Figure 50. GRK subfamily of AGC kinases. **(a)** GRK1 subfamily. **(b)** GRK2 subfamily. **(c)** GRK4 subfamily. Lipid modifications are shown in orange, plusses indicate the positively charged membrane binding region

GRK1 subfamily employs lipid modifications for interaction with the membrane. The CaaX consensus (where 'a' is an aliphatic amino acid) is either farnesylated in GRK1 (Inglese, Koch, Caron, & Lefkowitz, 1992) or geranylgeranylated in GRK7 (C. K. Chen *et al.*, 2001a; Hisatomi *et al.*, 1998). GRK2 and GRK3 have a C-terminal pleckstrin homology (PH) domain that interacts with the Gβγ subunit of G-proteins that, in turn, targets the kinase to the membrane (Pitcher *et al.*, 1992). GRK4, GRK5 and GRK6 have a positively charged region in their N-terminus that binds PIP_2 (Pitcher *et al.*, 1996). In addition, GRK4 and GRK6 can be palmitoylated (Premont, Macrae, Stoffel, & Chung, 1996; Stoffel, Randall, Premont, Lefkowitz, & Inglese, 1994) and GRK5 has a unique positively charged C-terminus that interacts with negatively charged membrane phospholipids (Pronin, Carman, & Benovic, 1998; Thiyagarajan *et al.*, 2004).

A.1.2 GRK6 structure

At the beginning of this project, the only determined crystal structures from the GRK4 subfamily were those of GRK6 in complex with AMPPNP, AMP, or sangivamycin, an adenosine analog. The crystal structure of GRK6 in complex with AMP and sangivamycin captured the kinase in a relatively closed conformation compared to previously determined structures of GRK1, GRK2, and GRK6 (Boguth, Singh, Huang, &

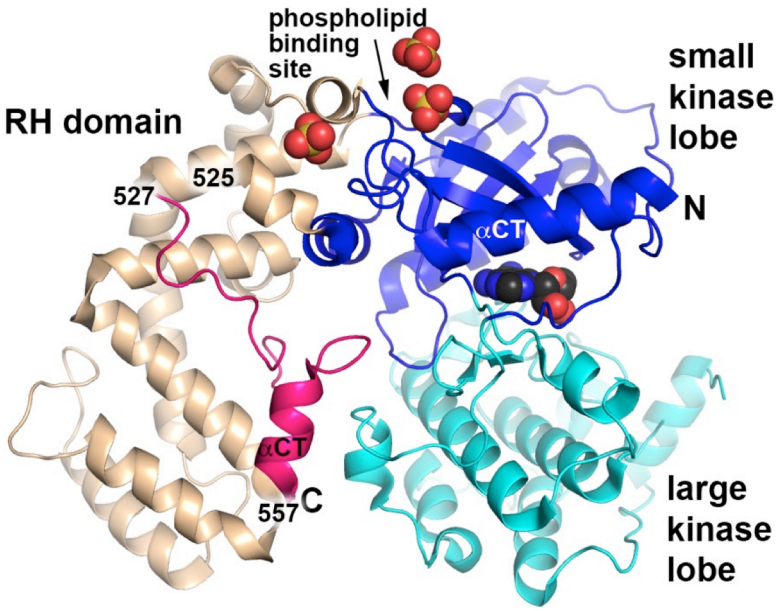

Figure 51. The structure of GRK6.The RH domain is shown in wheat, small kinase lobe in blue, large kinase lobe in cyan. The C-terminal amino acids 526-557 from the adjacent chain are in magenta. Three sulfate ions bound in the putative PIP_2 binding site and sangivamycin are shown as spheres.

Tesmer, 2010; Lodowski, Tesmer, Benovic, & Tesmer, 2006; Singh, Wang, Maeda, Palczewski, & Tesmer, 2008; V. M. Tesmer, Kawano, Shankaranarayanan, Kozasa, & Tesmer, 2005). The kinase domain is split into two parts – small and large lobes which require an additional rotation of 7° in order to achieve what is anticipated to be the fully closed, active conformation (Fig. 51) based on the active conformation of PKA (Madhusudan, Akamine, Xuong, & Taylor, 2002). Because GRKs are expected to adopt a closed conformation when they form a complex with an activated GPCR, these GRK6 structures also represent the most active GRK conformation crystallized to date. As opposed to the previous GRK6 structure in complex with AMPPNP, the GRK6 N-terminus is nearly fully ordered up to residue 557 near its C-terminus. Because most of the phospholipid-binding sites are ordered in this structure, it can serve as a model for predicting the possible GRK orientation at the membrane and GPCRs.

The first 17 amino acids from the N-terminus of GRK6 comprise an amphipathic helix with a hydrophobic interface facing outwards from the protein core. Similarly to the previously determined crystal structure of opsin with a peptide derived from the C-terminus of transducin, where the hydrophobic surface of the peptide makes contacts with the transmembrane helix 5 and 6 of opsin (Scheerer *et al.*, 2008), we predicted that the hydrophobic surface of the GRK6 N-terminal helix will serve as a docking site for

GPCRs. This would bring the flat positively charged surface made of amino acids 22-29, corresponding to the predicted N-terminal phospholipid binding site (Pitcher *et al.*, 1996), to an ideal position for binding the negatively charged surface of membrane phospholipids. This surface could therefore serve as an additional anchoring point for GRK6 to reinforce its binding to the receptor. Furthermore, three sulfate anions, derived from the crystallization solution, were bound to GRK6 in its crystal structure. The anions formed contacts with Lys28, Lys29, Arg31, Asn184 and Arg206 are believed to emulate PIP_2 binding.

The ordered C-tail of GRK6 forms an amphipathic helix that is domain swapped between two monomers of a GRK6 non-crystallographic dimer, and docks between the RH domain and the large lobe of the kinase domain. This, however, likely represents a crystallographic artifact, as GRK6 is monomeric in solution. However, it is reasonable to predict that the highly flexible linker connecting the kinase domain and C-terminal amphipathic helix could allow this binding site to be occupied with the C-terminus coming from the same GRK6 molecule when in solution. If so, the second predicted phospholipid binding site (amino acids 552-562 for GRK5 (Pronin *et al.*, 1998)) and cysteine residues known to undergo palmitoylation in GRK6 (Stoffel *et al.*, 1994) are quite far from the predicted membrane surface as defined by the N-terminal helix and sulfate ions described above. However, because the GRK6 C-tail is very flexible, it is possible that it might adopt multiple conformations dependent on the environment of the protein, on the palmitoylation state, and on the activation status of the kinase domain.

A.1.3 GRK5 interaction with membranes

GRK5 is the only member of GRK4 subfamily that relies solely on electrostatic interactions for membrane binding. The predicted amphipathic helix located at the C-terminus of GRK5 (amino acids 552-562) is expected to be an important phospholipid-binding determinant (Fig. 52). As such, membrane association of the GRK5 truncation mutant 1-551 was completely abolished, while 1-562 truncation had the same distribution as the full length protein (Pronin *et al.*, 1998). Moreover, mutations of residues on either hydrophobic (L550A, L551A, L554A, F555A) or positively charged (K547A, K548A, K556A and R557A) faces of the amphipathic helix also led to a complete loss of GRK5 plasma membrane localization in HEK293 cells (Thiyagarajan *et*

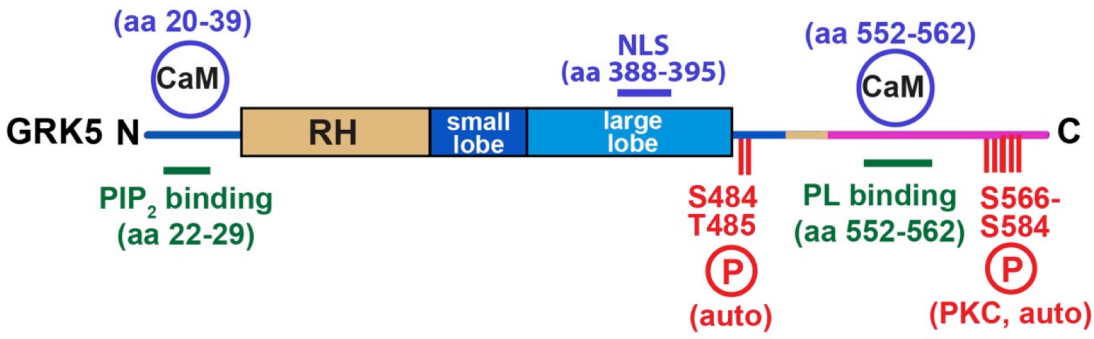

Figure 52. GRK5 regulatory sites. aa – amino acid, auto – autophosphorylation site, CaM – calmodulin binding site, NLS- nuclear localization sequence, PKC – protein kinase C phosphorylation site, PL – phospholipids.

al., 2004). Phospholipids also promote GRK5 autophosphorylation on residues of a "turn motif" S484 and T485, located in small kinase lobe. Autophosphorylation is required for full GRK5 receptor phosphorylation (Kunapuli, Gurevich, & Benovic, 1994a).

As in GRK6, GRK5 also has a binding site for PIP_2 near its N-terminus (amino acids 22-29), located immediately after its expected N-terminal helix. PIP_2 is also required for GRK5 membrane binding and receptor phosphorylation. In addition to PIP_2, phosphatidylinositol 4-phosphate can support β2 adrenergic phosphorylation by GRK5, albeit with less efficiency (Pitcher *et al.*, 1996). Since PIP_2 binding affects the catalytic activity through membrane binding, it has no effect on the peptide phosphorylation.

A.1.4 GRK5 regulation by Ca^{2+}-CaM

All GRKs bind calmodulin (CaM) in a Ca^{2+}-dependent manner (Chuang, Paolucci, & De Blasi, 1996; Pronin, Satpaev, & Slepak, 1997), however, affinities for GRK4 subfamily members are the highest (50 nM for GRK5 vs 2 μM for GRK2) (Pronin *et al.*, 1997). GRK5 has two distinct CaM-binding sites that overlap with its PIP_2- (amino acids 20-39) or phospholipid (amino acids 552-562) binding regions. It seems therefore that both sites are independent of one another and could, potentially, each bind a CaM molecule with the resulting stoichiometry 2:1 for CaM:GRK5. However it is still unclear how many CaM molecules are actually bound per one GRK5 (Levay, Satpaev, Pronin, Benovic, & Slepak, 1998). Binding to CaM results in GRK5 dissociation from the membrane and inhibits receptor phosphorylation, without affecting the phosphorylation of soluble substrate casein(Chuang *et al.*, 1996; Pronin *et al.*, 1997).

CaM binding also promotes autophosphorylation of GRK5 near it C-terminus within the 579-584 amino acid region (at sites distinct from the ones engaged in phospholipid-induced autophosphorylation) (Pronin *et al.*, 1998). This region immediately follows the PKC-dependent phosphorylation sites (within amino acids 566-572) (Pronin & Benovic, 1997). PKC-dependent phosphorylation or Ca^{2+}-CaM-dependent autophosphosphorylation both lead to inhibition of GRK5 –dependent rhodopsin phosphorylation without affecting its binding to phospholipid membranes. Considering that PKC activation and rise in Ca^{2+} levels both happen within the same regulatory pathway after phospholipase C activation (Jalili, Takeishi, & Walsh, 1999), it is likely that GRK5 C-tail phosphorylation serves to prolong the signaling occurring through Gq-coupled GPCRs.

A.1.5 GRK5 in hypertension and chronic heart failure.

GRK5 is ubiquitously expressed in human tissues, but the highest levels of expression are found in retina, lungs and heart (Premont, Koch, Inglese, & Lefkowitz, 1994). GRK5 has many known GPCR targets including rhodopsin, the β_1- and β_2-adrenergic receptors, the M_2 muscarinic receptors, and the angiotensin 1A receptor (Freedman *et al.*, 1995; Hu, Chen, Premont, Cong, & Lefkowitz, 2002; Kunapuli, Onorato, Hosey, & Benovic, 1994b; Oppermann, Freedman, & Alexander, 1996; Premont *et al.*, 1994; Rockman *et al.*, 1996; Tran, Jorgensen, & Clark, 2007). Together with GRK2, GRK5 is implicated in the development of heart failure. Even though GRK5 knockout mice are viable and do not have significant abnormalities in their physiology or behavior (as opposed to GRK2 knockout mice that die in embryonic stages (Jaber *et al.*, 1996)), they show cholinergic supersensitivity and impaired muscarinic receptor desensitization that results in hypothermia, hypoactivity, tremor and salivation (Gainetdinov *et al.*, 1999). In contrast, GRK5 overexpression in transgenic mouse models leads to marked β-adrenergic receptor desensitization (Rockman *et al.*, 1996), decreased cardiac output and contractility (E. P. Chen, Bittner, Akhter, Koch, & Davis, 2001b) and exaggerated hypertrophy and early heart failure compare to control mice after pressure overload (Martini *et al.*, 2008). It is also suggested that this kinase can be at least partially responsible for changes in myocardial function during heart failure(E. P. Chen *et al.*, 2001b).

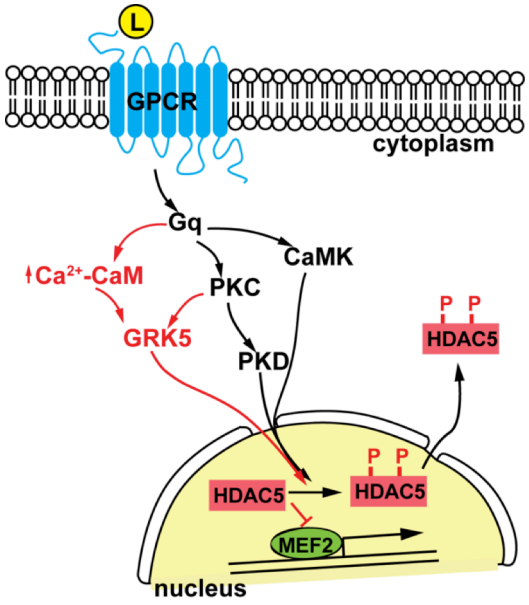

Figure 53. Putative signaling cascade leading to a hypertrotrophic response upon GPCR activation.

In addition to GPCR phosphorylation, GRK5 can initiate G-protein independent pathways during hypertrophic response (Fig. 53). Residues 388-395 located in the

kinase domain of GRK5 compose a nuclear localization sequence (NLS), responsible for a constitutive nuclear presence of GRK5 (Johnson, Scott, & Pitcher, 2004), however, an even greater nuclear accumulation of GRK5 in cardiomyocytes has been observed in spontaneously hypertensive heart failure rats (Yi, Gerdes, & Li, 2002), during the hypertrophic response to pressure overload (Martini *et al.*, 2008) or after myocyte stimulation with Gq-coupled receptor agonists, phenylephrine or angiotensin II (Gold *et al.*, 2013). Nuclear accumulation of GRK5 is dependent on Ca^{2+}-CaM binding at the N-terminal site following Gq cascade activation. After nuclear translocation GRK5 is able to phosphorylate histone deacetylase-5 (HDAC5), a myocyte enhancer factor-2 (MEF2) repressor (Martini *et al.*, 2008). Phosphorylation leads to HDAC5 export from the nucleus and transcription of MEF2-associated hypertrophic genes (S. Chang *et al.*, 2004; McKinsey, Zhang, Lu, & Olson, 2000; C. L. Zhang *et al.*, 2002). All of this data leads to the hypothesis that nuclear localization of GRK5 is involved in cardiac hypertrophy that results from chronic hypertension.

A.2 Results

A.2.1 GRK5 crystallization

The primary goal of this project was to determine the crystal structure of GRK5, a member of GRK4 subfamily involved in the regulation of cardiac signaling. Although the structure of the closely related GRK6 has been solved previously in our laboratory (Boguth *et al.*, 2010; Lodowski *et al.*, 2006), the structure of GRK5 was expected to be beneficial for rational drug design to explore new therapeutics against heart disease. In addition, we hoped to gain understanding in how the N- and C-termini of GRK5 regulate its membrane orientation, specifically, if the C-terminus of GRK5 makes similar contacts with the RH domain as the C-terminus of GRK6 when in its mostly closed conformation (Boguth *et al.*, 2010).

For crystallization trials we worked with bovine full length GRK5 ($GRK5_{FL}$, amino acids 1-590) and its C-terminal truncations, 1-561 ($GRK5_{561}$) and 1-531 ($GRK5_{531}$). $GRK5_{561}$ corresponds to the ordered portions of GRK6 in its active conformation, ending immediately after the αCT helix (Fig. 51) (Boguth *et al.*, 2010) and $GRK5_{531}$ is modeled after the GRK6·AMPPNP complex, which had less order in the C-terminus. All GRK5 mutants were cloned into pFastBacDual vector and purified as described (P. Yang, Glukhova, Tesmer, & Chen, 2013).

First, we tested the ability of each of the GRK5 constructs to phosphorylate rhodopsin, the model substrate for GRKs. For this, 100 nM GRK5 was mixed with various concentrations of rod outer segment (ROS) in a buffer containing 20 mM HEPES pH 7.5, 4 mM $MgCl_2$ and 2 mM EDTA and incubated for 30 min at 20 °C in the dark. The reaction was started by simultaneous exposure to light and the addition of ATP (containing trace amounts of [$^{32}\gamma$P] ATP) to a final concentration of 1 mM. At 3, 4 and 5 min the samples were quenched with SDS-PAGE loading dye. Following separation, gels were dried, exposed with a phosphorimager screen and scanned on a Typhoon scanner. The bands were quantified using the Image Quant software. To determine kinetic parameters, the initial velocities were calculated from the linear fit of

the data collected at different time points, followed by plotting these slopes against different ROS concentrations. The curve was fit using the Michaelis-Menten equation.

Table 9. Activity of different GRK5 mutants towards ROS

	$GRK5_{FL}$	$GRK5_{561}$	$GRK5_{531}$
k_{cat}, min^{-1}	2.5±0.4	5.9±0.8	3.3±0.7
K_M, μM	6.9±3.2	8.3±3.3	12.5±6.3
k_{cat}/K_M, $min^{-1}\cdot\mu M^{-1}$	0.4±0.2	0.7±0.3	0.3±0.1

Numbers represent the averages and standard deviations of at least three independent experiments

All tested GRK5 constructs seem to have similar affinity for rhodopsin and comparable k_{cat} values (Table 9). However, $GRK5_{561}$ was more active compared to $GRK5_{FL}$ and $GRK5_{531}$ (5.9 min^{-1} vs. 2.5 min^{-1} and 3.3 min^{-1}, respectively). This result is consistent with previous studies, where it has been suggested that the extreme C-terminal region of the GRK4 subfamily (amino acids 563-590 in GRK5) serves an autoinhibitory function in receptor phosphorylation (Pronin *et al.*, 1998; Vatter, Stoesser, Samel, Gierschik, & Moepps, 2005). Further truncation to $GRK5_{531}$ also deleted the phospholipid-binding site (amino acids 552-562), presumably, leading to the restoration of its activity to the level of $GRK5_{FL}$.

Next, we compared melting temperatures of GRK5 constructs in the presence or absence of different ATP and adenosine analogs. For this experiment, we mixed 0.1 mg/ml of GRK5 with 0.1 mM 1-anilinonaphthalene- 8-sulfonic acid (ANS) in 20 mM HEPES pH 8.0, 200 mM NaCl and 2 mM DTT. Then we added 2.5 mM $MgCl_2$ along or with 5 mM ATP, ADP or AMPPNP or with 0.4 mM sangivamycin. After 30 min incubation at 4 °C, samples were heated from 4 to 85 °C at 1 ˚C/min in a ThermoFluor Analyzer (Johnson & Johnson). Plate fluorescence was measured in 1 °C intervals, using a 475-525 nm emission filter. T_m values were calculated as the inflection point of the melting curve using the instrument software.

The resulting melting temperatures of the GRK5 variants were nearly identical and strongly depended on the bound ligand (Table 10). Melting temperatures of GRK5 in the presence of $MgCl_2$ alone were around 31 °C. Sangivamycin shifted GRK5 melting

temperatures by about 2 °C, ADP and AMPPNP by 3.5 °C. ATP caused the greatest

Table 10. Stability of GRK5 truncation mutants by ThermoFluor, in °C

	Mg^{2+}	Mg^{2+} +ATP	Mg^{2+} +ADP	Mg^{2+} +AMPPNP	sangiva-mycin
$GRK5_{FL}$	31.3±0.1	38.5±0.2	34.5±1.4	34.6±0.3	33.2±0.1
$GRK5_{561}$	31±0.1	38.7±0.2	34.8±0.4	34.4±0.1	33.3±0.1
$GRK5_{531}$	31.3±0.2	38.4±0.2	35.2±0.4	34.3±0.2	33.6±0.2

Numbers represent the averages and standard deviations of at least three independent experiments

shift of 7.5 °C, relative to GRK5 with $MgCl_2$ alone.

We have performed crystallization trials with all aforementioned GRK5 constructs with and without all mentioned ATP analogs at 4 and 20 °C. However no crystals have been produced. Various mutations of GRK5, such as S484D/T485D (mutant mimicking autophosphorylation (Premont *et al.*, 1994)), M165K (mutation designed to disrupt potential crystallographic dimer interface, analogous to L166K mutant of GRK1 (J. J. G. Tesmer, Nance, Singh, & Lee, 2012)), K389A/E390A/K391A or Q435A/E436A/K391A (surface entropy reduction mutations predicted by UCLA MBI — SERp Server (Goldschmidt, Cooper, Derewenda, & Eisenberg, 2007)) also yielded no crystallization hits.

A.2.2 GRK5 interaction with Ca^{2+}/Calmodulin

We were also interested in the GRK5 interaction with Ca^{2+}/Calmodulin (Ca^{2+}/CaM) for two reasons. First, the complex of GRK5 with CaM is stable and may represent a better target for crystallization. Second, because many details of how GRK5 is regulated by CaM are unknown, we wanted to use biochemical and crystallographic approach to answer these questions and in particular how CaM binds to two distinct GRK5 CaM-binding sites, and what consequences it has on the overall GRK5 structure.

The pACYC/trc-hCaM plasmid expressing human calmodulin was a generous gift from R. Neubig laboratory. CaM was expressed and purified as previously described (H. Li *et al.*, 2008). First, we confirmed that purified Ca^{2+}/CaM interacts with $GRK5_{FL}$ and

inhibits its phosphorylation of ROS. For this, we performed GRK5 activity assays (described above) in the presence of 5 μM ROS, 80 mM $CaCl_2$ and increasing CaM concentrations (Fig. 54). An IC_{50} value of 2 μM was obtained from the "log (inhibitor) vs. response" fit in Prism software and was converted to K_i (40nM) using the Cheng-Prusoff equation. The obtained IC_{50} values for Ca^{2+}/CaM are 40-fold higher than ones reported previously (Chuang *et al.*, 1996; Pronin *et al.*, 1997) and, probably, reflect differences in assay conditions, in particular, the ROS and GRK5 concentrations.

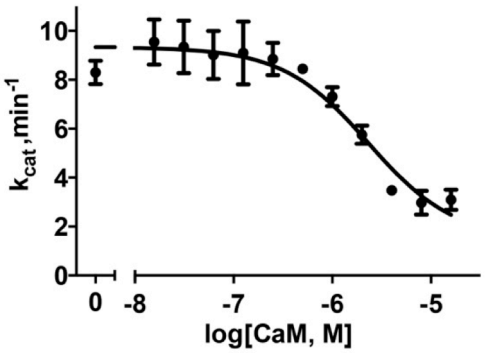

Figure 54. Inhibition of $GRK5_{FL}$ activity by Ca^{2+}/CaM.

Next, we made complexes between Ca^{2+}/CaM and $GRK5_{FL}$ or $GRK5_{531}$ and examined them using multi-angle light scattering (MALS). For this we mixed 132 μg of GRK5 variants with 120 μg of CaM (1:10 molar ratio of GRK5:CaM) in 20 mM HEPES pH 8.0, 100 mM NaCl, 2mM DTT, and 10 mM $CaCl_2$, incubated them for 30 min at 4 °C and separated using silica-gel size exclusion column connected to Dawn Helios II multi-angle light scattering instrument. The UV absorption traces and corresponding molecular weights calculated based on the light scattering are shown in Fig. 55. When separated using size-exclusion chromatography, GRK5 eluted at an abnormally low molecular weight of 30 kDa, presumably due to its interaction with the resin. Molecular weight as determined by light scattering, however, corresponded to 65 and 75 kDa for $GRK5_{531}$ and $GRK5_{FL}$, respectively (similar to their calculated molecular weights of 62 and 68 kDa). Upon the addition of excess CaM, new peaks corresponding to complexes of Ca^{2+}/CaM·GRK5 emerge with molecular weights of 78 and 88 kDa for the Ca^{2+}/CaM·$GRK5_{531}$ and Ca^{2+}/CaM·$GRK5_{FL}$ complexes, respectively. The molecular weight of CaM was measured to be 18 kDa (similar to its calculated molecular weight of 16.7 kDa). CaM lacks tryptophan residues and thus the excess CaM peak had a very modest absorbance at 280 nm compared to GRK5 (Fig. 55). Peak analysis by SDS-PAGE confirmed the presence of both GRK5 and CaM in the complex fractions (data not shown).

Thus, both $GRK5_{531}$ and $GRK5_{FL}$ were able to form complexes with CaM. Interestingly, $GRK5_{FL}$ seems to bind only one molecule

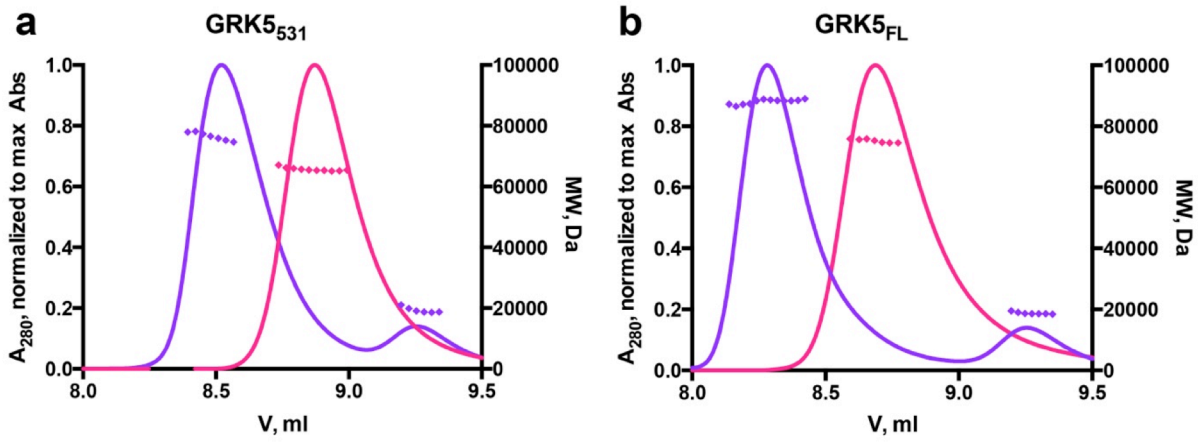

Figure 55. Multi-angle light scattering of GRK5 variants by themselves and in complex with Ca^{2+}/CaM. **(a)** $GRK5_{531}$. **(b)** $GRK5_{FL}$. Elution profiles of GRK5 in the absence of CaM is shown in pink, and that of Ca^{2+}/CaM·GRK5 complex is in purple. Diamonds indicate the actual molecular weight measured by light scattering (right axis).

of CaM despite the fact that CaM is in vast excess over GRK5.

There are at least three explanations for 1:1 binding. First, the tested CaM concentration might have not been enough to saturate both CaM-binding sites. However, this is unlikely because the final CaM concentration in the sample was 110 μM, 500-fold higher then the reported K_D for the low affinity CaM site (200 nM for the N-terminal CaM-binding site). Secondly, the N- and C-terminal CaM binding sites could be in close proximity to each other, in such way that CaM interaction with one site sterically prevents the binding of a second CaM molecule to the other. The third possibility is a noncanonical Ca^{2+}/CaM·GRK5 interaction, wherein one CaM molecule could interact simultaneously with both GRK5 binding sites, similar to the CaM interaction with two peptides derived from plant glutamate decarboxylase (Yap, Yuan, Mal, Vogel, & Ikura, 2003).

Previously, the affinities of the individual CaM-binding sites in GRK5 were measured using GST-fusions of GRK5-derived peptides, amino acids 1-200 or 20-39 for the N-terminal binding site and amino acids 489-590 for the C-terminal site (Levay *et al.*, 1998). Such dramatic truncations could lead to misfolded peptides and, thus,

measurement of their CaM-binding affinities may not reflect the actual affinities of the sites when presented within full length GRK5.

To determine the relative CaM binding affinities for the two separate sites in the context of full length GRK5 we used the flow cytometry protein interaction assay

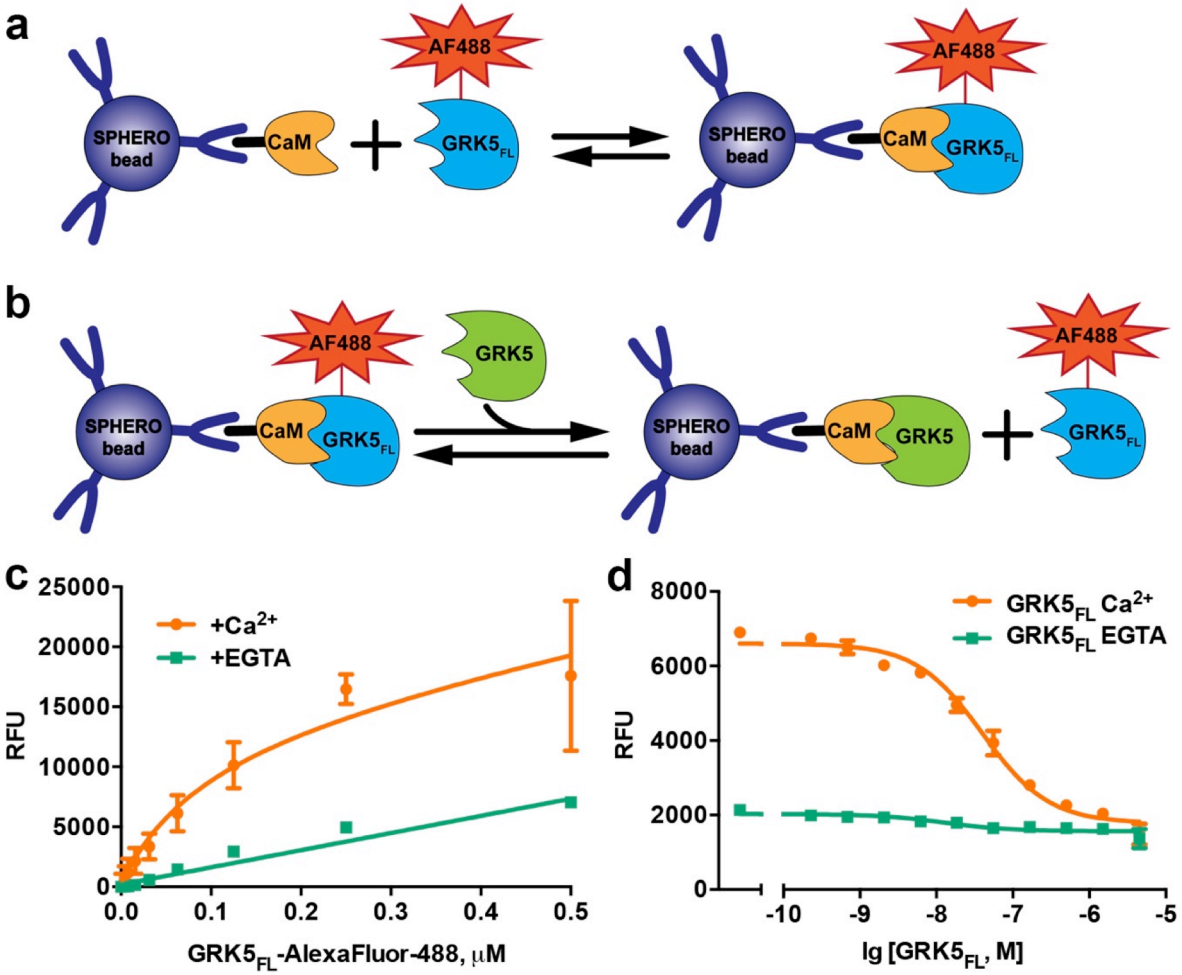

Figure 56. Determination of GRK5 binding affinity for Ca^{2+}/CaM by flow cytometry protein interaction assay. **(a)** Scheme for the direct binding assay of AlexaFluor-488-labeled $GRK5_{FL}$ and CaM, bound to SPHERO beads through biotin-streptavidin interaction. **(b)** Scheme for the competition assay. Unlabeled GRK5 competes with AlexaFluor-488-labeled $GRK5_{FL}$ for CaM binding, leading to its dissociation from the bead-bound CaM. **(c)** Typical binding curves from the direct binding assay between AlexaFluor-488-labeled $GRK5_{FL}$ and CaM in the presence of Ca^{2+} or EGTA. **(d)** Competition between unlabeled $GRK5_{FL}$ and between AlexaFluor-488-labeled $GRK5_{FL}$ for CaM binding in the presence of Ca^{2+} or EGTA.

(FCPIA) (Roman, Ota, & Neubig, 2009; Shankaranarayanan et al., 2008). First, we have determined the affinity of the full-length GRK5 for Ca^{2+}/CaM in a direct binding assay

(Fig. 56a). For this we labeled CaM with amine-reactive biotin at a 1:1 molar ratio, followed by its conjugation to SPHERO streptavidin-coated beads (Spherotech). Different amounts of $GRK5_{FL}$, labeled with AlexaFluor-488 C_5-maleimide (AF488-$GRK5_{FL}$) at 1:1 ratio, were incubated with CaM-beads in the buffer containing 20 mM HEPES pH 8.0, 100 mM NaCl, 2 mM DTT, 1% (w/v) bovine serum albumin (BSA) and 0.1% (v/v) lubrol containing either 2.5 mM EGTA or 2.5 mM $CaCl_2$ for 30 min at 20 °C. Then, the bead-associated fluorescence was measured using Accuri C6 Flow Cytometer. We plotted the fluorescence as a function of AF488-$GRK5_{FL}$ concentration and fit the curve using an equation for total and non-specific binding in GraphPad Prism software. A representative curve is shown in Fig. 56c. As can be seen, AF488-$GRK5_{FL}$ binding to CaM was strictly dependent on the presence of Ca^{2+} ions. When EGTA was present, only linear nonspecific binding of $GRK5_{FL}$ to the beads could be observed. In the absence of both Ca^{2+} and EGTA, the curves look identical to the EGTA control (data not shown). The K_D of CaM for GRK5 was thereby determined to be 100 nM.

For competition experiments, various concentrations of unlabeled GRK5 variants or peptides were incubated with 10 nM of CaM-conjugated beads and 100 nM of AF488-$GRK5_{FL}$. Peptides that bind CaM were able to compete with fluorescent $GRK5_{FL}$ leading to a decrease in bead-associated fluorescence compared to the samples in which no competitor was present (Fig. 56b). A representative experiment is shown in Fig. 56d. In the presence of Ca^{2+}, both AF488-$GRK5_{FL}$ and $GRK5_{FL}$ bind CaM, but at high concentrations $GRK5_{FL}$ outcompetes AF488-$GRK5_{FL}$ for CaM binding, resulting in a low fluorescence signal. When EGTA is present, only low levels of fluorescence could be observed. For IC_{50} calculations the fluorescence values in the presence of EGTA were subtracted from the ones in the presence of Ca^{2+}, and the curves were fit using "log (inhibitor) vs response" equation in Prism.

Table 11 shows the IC_{50} values from competition FCPIA experiments described above and K_i values calculated using the Cheng-Prusoff equation (shown are the averages and standard deviations of at least three independent experiment for each peptide). K_i for $GRK5_{FL}$ was 45 nM, agreeing reasonably well with the previously reported data for K_D of the $GRK5_{FL}$-CaM complex (8 nM) (Levay *et al.*, 1998). The K_i of $GRK5_{561}$ resembled that of $GRK5_{FL}$, supporting the fact that the extreme C-terminus is

not important for CaM binding. GRK5 truncation past the C-terminal site resulted in a significant decrease of affinity for CaM (334 nM for $GRK5_{531}$). We have also tested $\Delta23GRK5_{531}$, a construct lacking its N-terminal helix (Boguth *et al.*, 2010), a predicted GPCR-interaction site, in addition to the C-terminal CaM-binding site. This construct had similar affinity for CaM (520 nM) as $GRK5_{531}$, indicating that the N-terminal helix is not important for CaM binding. We also made a $GRK5_{FL}$ construct wherein the positively charged amino acids of the N-terminal CaM –binding site were mutated to alanine, $GRK5_{NT}$ (K26/28/29/31/35A). The $GRK5_{NT}$ affinity for CaM (110 nM) was also significantly reduced compared to $GRK5_{FL}$ or $GRK5_{561}$, suggesting that the presence of both sites are required for high affinity binding between GRK5 and CaM. GRK6 affinity for CaM was significantly lowered then that of GRK5, despite its high sequence similarity within the predicted CaM-binding regions.

Table 11. IC_{50} and K_i of various GRK5 constructs determined by FCPIA assay:

GRK5 constructs	IC_{50}	K_i
proteins		
$GRK5_{FL}$	90 ± 53 nM	45 ± 26 nM
$GRK5_{561}$	35 ± 10 nM	17 ± 5 nM
$GRK5_{531}$	667 ± 309 nM	334 ± 154 nM
$_{\Delta23}GRK5_{531}$	1.1 ± 0.4 μM	0.52 ± 0.2 μM
$GRK5_{NT}$	222 ±80 nM	110 ±40 nM
GRK6	>>15 μM	>>8 μM
peptides		
$GRK5_{2-31}$	336 ± 48 nM	168 ± 24 nM
$GRK5_{6-31}$	500 ± 379 nM	250 ± 190 nM
$GRK5_{10-31}$	1.4 ± 0.9 μM	0.7 ± 0.45 μM
$GRK5_{20-38}$	55 ± 16 nM	27 ± 8 nM
$GRK5_{2-24}$	>50 μM	>25 μM
$GRK5_{546-565}$	1.6 ± 0.1 μM	0.8 ± 0.03 μM

Numbers represent the averages and standard deviations of at least three independent experiments

We also tested the short peptides $GRK5_{2-31}$, $GRK5_{6-31}$, $GRK5_{10-31}$, $GRK5_{20-38}$, $GRK5_{2-24}$ and $GRK5_{546-565}$ for their CaM binding affinity (Table 11). Only the peptide corresponding to the N-terminal CaM- binding site, $GRK5_{20-38}$ bound CaM with high affinity (55 nM), whereas the $GRK5_{546-565}$ peptide containing the C-terminal site was a very weak CaM binder. The peptide affinity data explains why the $GRK5_{NT}$ construct loses CaM binding affinity, but it does not explain why C-terminally truncated $GRK5_{531}$ is also deficient in CaM binding. It is possible that the $GRK5_{546-565}$ peptide does not include all determinants required for high-affinity binding between the GRK5 C-terminal site and CaM.

Next we investigated the effect of CaM interaction on the $GRK5_{2-31}$, $GRK5_{25-31}$, $GRK5_{2-24}$ and $GRK5_{546-565}$ membrane association using sum frequency generation (SFG) vibrational spectroscopy and attenuated total reflectance−Fourier transform infrared (ATR-FTIR) spectroscopy in a collaboration with Z. Chen laboratory (Ding *et al.*, 2014). Out of all the peptides tested, only $GRK5_{2-31}$, $GRK5_{25-31}$ and $GRK5_{546-565}$ were able to interact with the POPC or POPC:PIP2 (9:1) membranes, whereas $GRK5_{2-24}$ could not, consistent with the role of the GRK N-terminal helix in receptor binding (Boguth *et al.*, 2010). $GRK5_{2-31}$ adopted a random coil orientation (Fig. 57a), however, it adopted a partially helical orientation in the presence of 40% tetrafluoroethylene (TFE). Interestingly, the membrane-bound orientation of the $GRK5_{2-31}$ helical segment

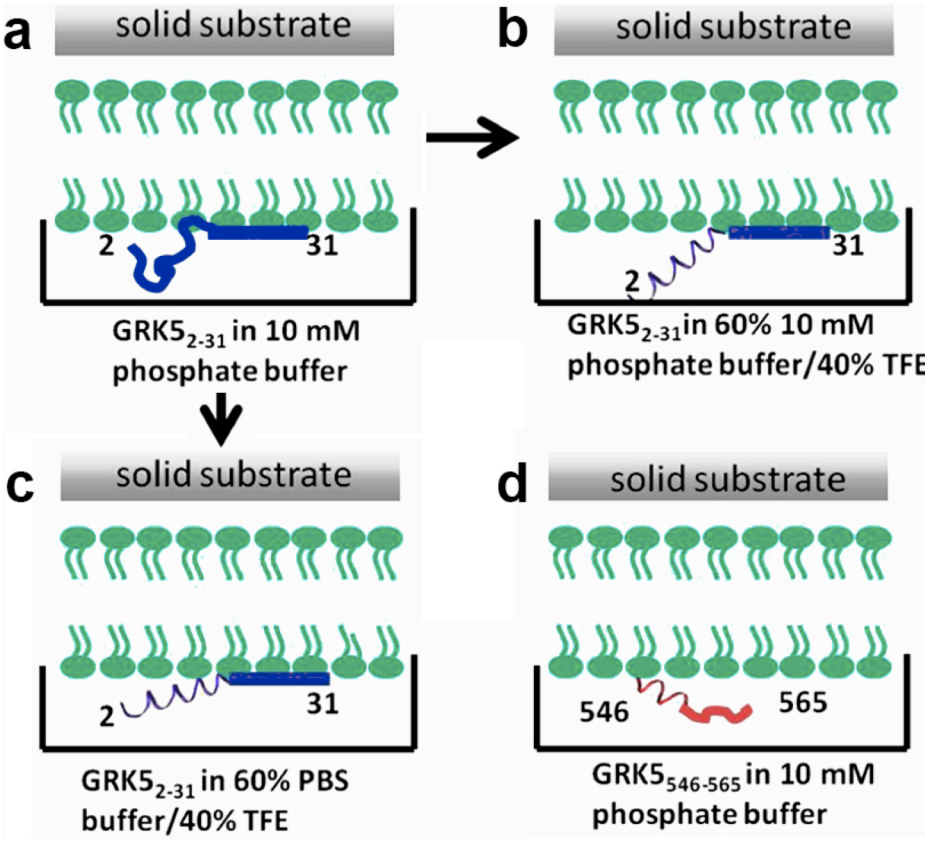

Figure 57. GRK5 peptide orientation when bound to model membranes. **(a)** $GRK5_{2-31}$ in 10 mM phosphate buffer pH 7.4 adopts a random coil orientation. **(b)** $GRK5_{2-31}$ is partially helical in 40% TFE/60% 10 mM phosphate buffer pH 7.4 **(c)** Membrane orientation of $GRK5_{2-31}$ in high ionic strength buffer (40% TFE/60% 4 mM phosphate buffer pH 7.4 and 155 mM NaCl) **(d)** $GRK5_{546-565}$ in 10 mM phosphate buffer pH 7.4 is partially helical. Modified from (Ding et al., 2014).

depended on the ionic strength of the buffer and was 46 ± 1° relative to the surface normal in 40% TFE/60% 10 mM phosphate buffer pH 7.4 but increased to 78 ± 11° in 40% TFE/60% PBS buffer (4 mM phosphate buffer pH 7.4 and 155 mM NaCl) (Fig. 57b and c). Addition of Ca^{2+}/CaM to the $GRK5_{2-31}$ peptide led to its extraction from the membrane judged by a decrease of ATR-FTIR signal. The $GRK5_{25-31}$ peptide was also strongly associated with the membrane although its orientation could not be determined due to lack of helical structure, and CaM addition did not decrease this interaction. Both $GRK5_{2-31}$ and $GRK5_{25-31}$ contain part of putative CaM binding site (amino acids 20-38), however $GRK5_{25-31}$ might simply be too short for efficient binding to CaM.

We also examined $GRK5_{546-565}$ for membrane and CaM binding. This peptide exhibited helical characteristics even in the absence of TFE, consistent with it forming a helix as observed in the GRK6·sangivamycin crystal structure (Boguth *et al.*, 2010). $GRK5_{546-565}$ was strongly associated with the membrane (Fig. 57d) and this interaction could be abolished by addition of Ca^{2+}/CaM, consistent with our peptide FCPIA data.

Thus, peptides containing either the N- or C-terminal CaM binding sites could be extracted from the membrane upon addition of Ca^{2+}/CaM, supporting the role of CaM as a regulator of GRK5 membrane association.

A.2.3 Structural analysis of GRK5 N- and C-termini

One possibility for the observed 1:1 binding ratio between GRK5 and CaM could be spatial proximity between the N-and C-termini. In the most active GRK6 conformation (PDB entry 3NYN), the C-terminal helix (αCT) is tucked between the RH domain and the large kinase lobe (Boguth *et al.*, 2010). However, it has been suggested that this structure represents an inactive GRK6 conformation because the αCT helix is sequestered and not in a position that would interact with a membrane surface.

First, we investigated if αCT docking between RH domain and the kinase large lobe is important for the GRK5 activity by making mutations that we predicted would destabilize this interaction (Fig. 58). We introduced the A88K/E89K mutations in the RH domain to eliminate van der Waals interactions between Ala88 and Leu537 and the salt bridge between Glu89 and Arg554; an R64A mutation to disrupt hydrogen bonds between the arginine guanidinium group and the carbonyl of L537; an L537A mutation to disrupt its hydrophobic interactions with A88 and L551; D536A and P546A mutations to interfere with the sharp turn before αCT; and M460K to test the importance of αCT interaction with the kinase large lobe.

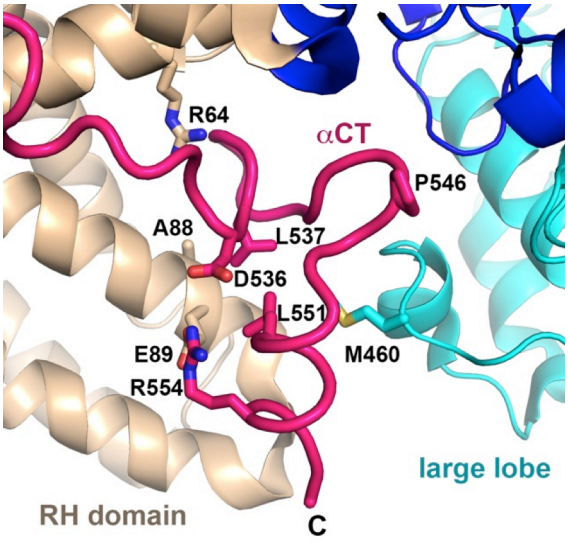

Figure 58. Localization of residues mutated to test the importance of aCT interaction with the RH domain and the kinase large lobe.

All mutations were introduced into $GRK5_{561}$ construct and their activity was measured using ROS as a substrate (Table 12). All mutants had similar affinity for ROS and comparable k_{cat} values. Only two mutants, D536A and L537A, had lower activity compared to $GRK5_{561}$, however this difference was less then 2-fold. Thus, it appears that αCT interactions with the RH domain and the kinase large lobe are not important

for GRK5 activity. It is possible, however, that αCT stabilizes the inactive conformation of the kinase. Unfortunately, no stability measurements were performed.

Table 12. Activity of $GRK5_{561}$ mutants

	$GRK5_{561}$	$GRK5_{561}$ A88K/E89K	$GRK5_{561}$ R64A	$GRK5_{561}$ M460K	$GRK5_{561}$ D536A	$GRK5_{561}$ L537A	$GRK5_{561}$ P546A
k_{cat},% of $GRK5_{561}$	96±7	89±17	160±34	87±22	58±9	62±9	140±16
K_M, μM	4.4±0.9	3.5±2.1	5.1±3	6.3±4.1	3.7±1.7	4.1±1.5	4.6±1.5
$kcat/K_M$,% of $GRK5_{561}\cdot\mu M^{-1}$	22±5	25±16	31±19	14±10	16±8	15±6	30±10

Numbers represent the averages and standard deviations of at least three independent experiments

Next, we decided to investigate the whether αCT localized close to either αNT or the RH domain using Forster resonance energy transfer (FRET). For this we created special GRK5 fusion constructs. An amino acid sequence, CCPGCC, capable of binding FlAsH reagent (Life technologies) with high affinity (Griffin, Adams, Jones, & Tsien, 2000), was introduced either before αNT ($GRK5_{561}N$) or between α4 and α5 of the RH domain in place of amino acids 94-96 ($GRK5_{561}45$) or between α6 and α7 in place of residues 136-138 ($GRK5_{561}67$). All constructs were fused to cyan fluorescent protein (CFP) at their C-terminus, creating $GRK5_{561}N$-CFP, $GRK5_{561}45$-CFP and $GRK5_{561}67$-CFP. The $GRK5_{561}45$-CFP protein exhibited very poor expression and was dropped from further analysis. $GRK5_{561}N$-CFP and $GRK5_{561}67$-CFP were expressed and purified, as described previously for $GRK5_{FL}$. All constructs had similar activity as $GRK5_{561}$ when assayed using the soluble substrate tubulin (data not shown). $GRK5_{561}N$-CFP, $GRK5_{561}67$-CFP were labeled with FlAsH using manufacturer's specifications, incorporating ~1 FlAsH per each GRK5, yielding $GRK5_{561}N_{FLASH}$-CFP and $GRK5_{561}67_{FLASH}$-CFP. Tubulin activity assays showed that $GRK5_{561}67_{FLASH}$-CFP was just as active as $GRK5_{561}$, but that $GRK5_{561}N_{FLASH}$-CFP retained only 30% of the $GRK5_{561}$ activity. However, more repeats of these experiments are necessary. No ThermoFluor assays could be performed due to the high background CFP fluorescence.

CFP emission spectra overlaps with FlAsH excitation spectra, thus, if CFP and FlAsH are spatially close; CFP excitation should lead to FlAsH fluorescence. Figure 59 depicts two potential scenarios leading to the FRET signal in our model system. First, if αCT were indeed tucked between the RH domain and the kinase domain, the CFP would be within the FRET distance from the FlAsH probe if the latter were located on the RH domain (as in $GRK5_{561}67_{FLASH}$-CFP). However, if the C-terminus changes its conformation to be in close proximity to the N-terminal PIP_2-binding site, then only FRET for the $GRK5_{561}N_{FLASH}$-CFP would be observed (Fig. 59). To monitor the FRET signal we excited the system at 425 nm and recorded fluorescence excitation spectra in the 450-600 nm range using a SpectraMax M5 fluorescent plate reader.

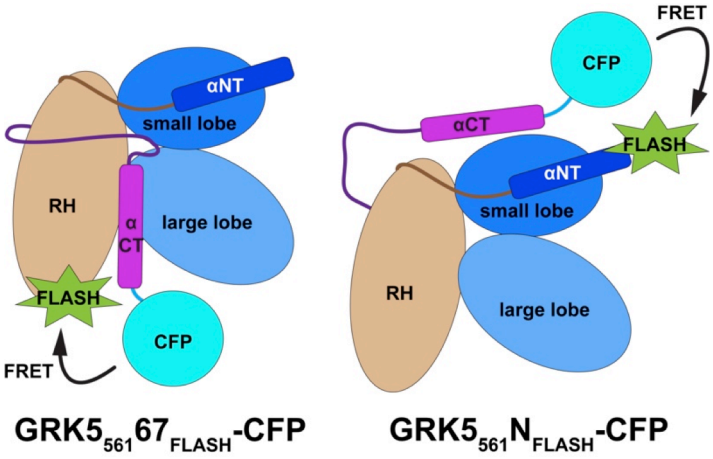

Figure 59. Schematics for $GRK5_{561}67_{FLASH}$-CFP and $GRK5_{561}N_{FLASH}$-CFP constructs. Shown are two possibilities for FRET signal observation.

Without FlAsH labeling, spectra of both GRK5$_{561}$N-CFP and GRK5$_{561}$67-CFP in a 20 mM HEPES 7.5, 150 mM NaCl and 10 mM β-mercaptoethanol (β-ME) buffer represent the excitation spectra for CFP alone, which exhibits a characteristic double peak (Fig. 60a and b, blue traces). When both FlAsH and CFP were present, a slight increase of fluorescence was observed at 530 nm, indicating FRET (Fig. 60a and b, green traces). The shoulder at 530 nm was present in both GRK5$_{561}$N$_{FLASH}$-CFP and GRK5$_{561}$67$_{FLASH}$-CFP constructs, presumably reflecting the fact that the αCT can adopt multiple orientations at high ionic strength.

It is well known, that salt inhibits GRKs and thus most activity assay are performed in very low ionic strength buffers. Thus, we investigated the effect of ionic

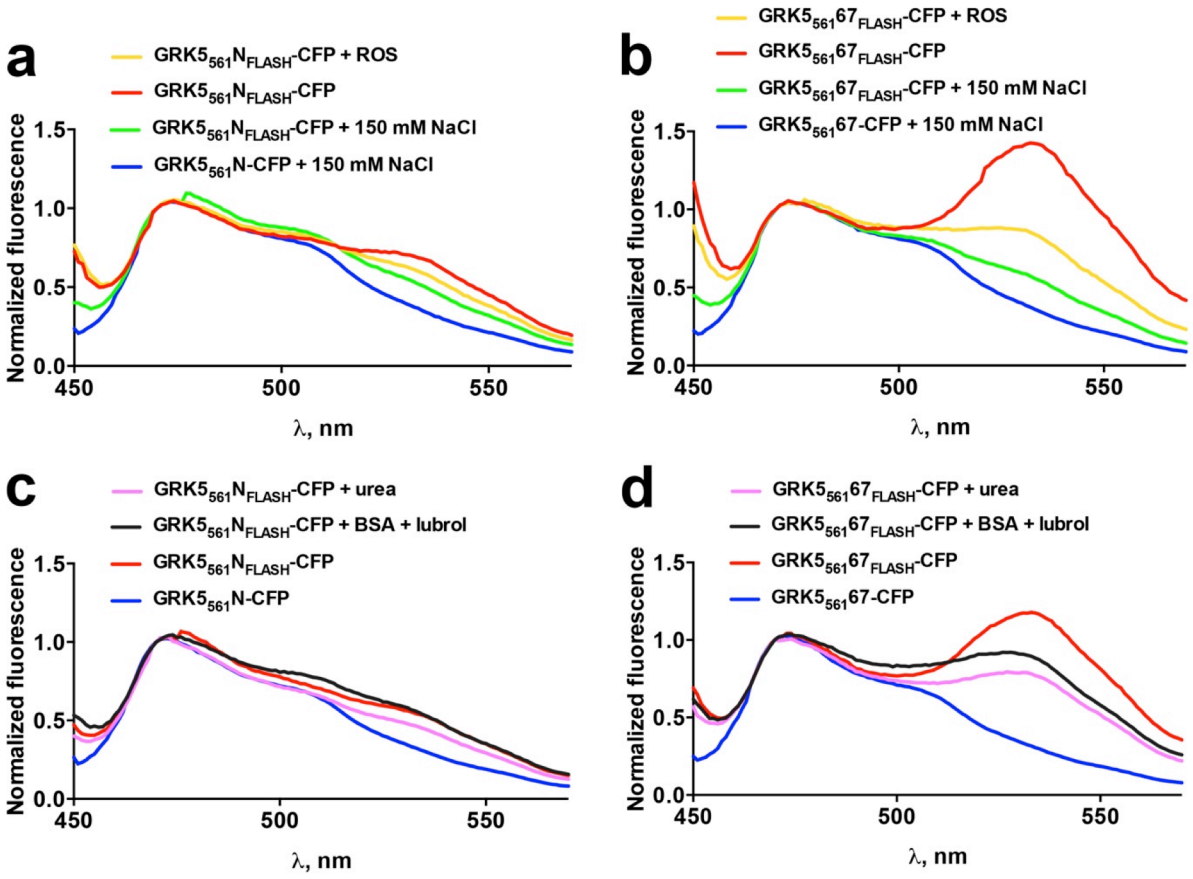

Figure 60. Fluorescent spectra of GRK5$_{561}$N$_{FLASH}$-CFP and GRK5$_{561}$67$_{FLASH}$-CFP under various conditions. Effect of the ionic strength and ROS on the FRET signal of **(a)** GRK5$_{561}$N$_{FLASH}$-CFP and **(b)** GRK5$_{561}$67$_{FLASH}$-CFP. Effect of the agents reducing the nonspecific binding on **(c)** GRK5$_{561}$N$_{FLASH}$-CFP and **(d)** GRK5$_{561}$67$_{FLASH}$-CFP.

strength on the FRET signal in our model system. For this we recorded the excitation spectra of $GRK5_{561}N_{FLASH}$-CFP and $GRK5_{561}67_{FLASH}$-CFP in a buffer containing 20 mM HEPES pH 7.5 and 10 mM β-ME (Fig. 60a and b, red traces). Whereas the FRET signal of $GRK5_{561}N_{FLASH}$-CFP increased only slightly, the FRET signal of $GRK5_{561}67_{FLASH}$-CFP was increased dramatically and was strongly dependent on the salt concentration. The presence of even 50 mM salt practically eliminated the FRET (data not shown). Addition of 5 μM ROS had similar effect, albeit of lower amplitude (Fig. 60a and b, red traces). Thus, it seems that in the absence of the GPCRs, the αCT is indeed localized between the RH domain and the large kinase lobe. However interaction with ROS (or, possibly, the membranes from the ROS preparation) dislodges the αCT.

Too determine if the observed high FRET signal for $GRK5_{561}67_{FLASH}$-CFP in the low ionic strength buffer was due to the nonspecific effects, we measured the same spectra in the presence of 1 M urea, 1% BSA, 0.1% lubrol or a combination of the last two (Fig. 60c and d). None of these agents appeared to have significant effect on FRET of $GRK5_{561}N_{FLASH}$-CFP, however, they reduced the FRET of $GRK5_{561}67_{FLASH}$-CFP but only by about 30%. Thus, it seems that the observed interaction between αCT and the RH domain is specific. However many more controls need to be done, to confirm that the observed FRET signal is indeed intramolecular and not occurring between different $GRK5_{561}67_{FLASH}$-CFP molecules. In addition, regarding the effect of ROS, it would be necessary to dissect the effect of the membrane vs. the GPCR itself. However, if the observed effect will prove to be genuine, such a model system could have great potential to study the structural rearrangements occurring in GRKs during their interactions with GPCR. Such a system could be applied both *in vitro* and *in vivo*, as FlAsH reagent permeates cell membrane and could be used to label living cells *in vivo* (Griffin *et al.*, 2000).

A.2.4 GRK5 membrane orientation

In a separate project we attempted to discern the roles of N- and C-termini of GRK5 in its membrane orientation using combined SFG and attenuated total reflectance-Fourier transform infrared spectroscopy (ATR-FTIR) in a collaboration with Zhan Chen laboratory (P. Yang *et al.*, 2013). This method has been used previously to determine the membrane orientation of GRK2-G$\beta\gamma$ complex (Boughton, Yang, & Tesmer, 2011). To determine the GRK5 orientation at the membrane, the SFG and ATR-FTIR data were combined and the crystal structures of GRK6 (2ACX and 3NYN) was used for data analysis and modeling, as the GRK5 crystal structure was not available at the time.

First we analyzed the membrane orientation of $GRK5_{FL}$ (Fig. 61a and b) on the negatively charged 1-palmitoyl-2-oleoyl-*sn*-glycero-3-phosphoglycerol (POPG) membranes. Analysis yielded two possible orientations of GRK5FL, twist=70°, tilt=2° and twist=340°, tilt=10°, which are closely related. The observed orientation placed the predicted N-terminal phospholipid-binding site (amino acids K26A, K28A, K29A, K31A, K35A) in close vicinity with the membrane.

Deletion of the GRK5 C-termini in $GRK5_{531}$ construct had no effect on GRK5 membrane orientation on POPG membranes (twist=40°, tilt=10° and twist=300°, tilt=26°) (Fig. 61c and d). PIP_2 incorporation into the experimental bilayer (1:1 molar ratio of PIP_2:POPG) also had no effect on its membrane orientation. Thus, it seems that the extreme C-terminus has no effect on the GRK5 membrane orientation.

Next, me mutated the residues predicted to be important for phospholipid binding at the N-terminus, creating $GRK5_{NT}$ (K26/28/29/31/35A). The melting temperature of $GRK5_{NT}$ was 3 °C lower then that of $GRK5_{FL}$, and its activity on the tubulin and ROS substrates was 50% and 100-180% of that $GRK5_{FL}$, respectively (though more repeats are necessary). When the membrane orientation of $GRK5_{NT}$ was assayed using combined SFG and ATR-FTIR technique, it was found that although this protein bound to the lipid bilayer, its orientation was stochastic.

Thus we concluded that the N-terminal phospholipid-binding site is the primary site responsible for specific binding to anionic phospholipids. The C-terminal site might

still bind to the membrane, but it does not impart a specific orientation. These results are consistent with previously reported data showing the importance of GRK5 C-terminus for the plasma membrane localization (Pronin *et al.*, 1998; Thiyagarajan *et al.*, 2004).

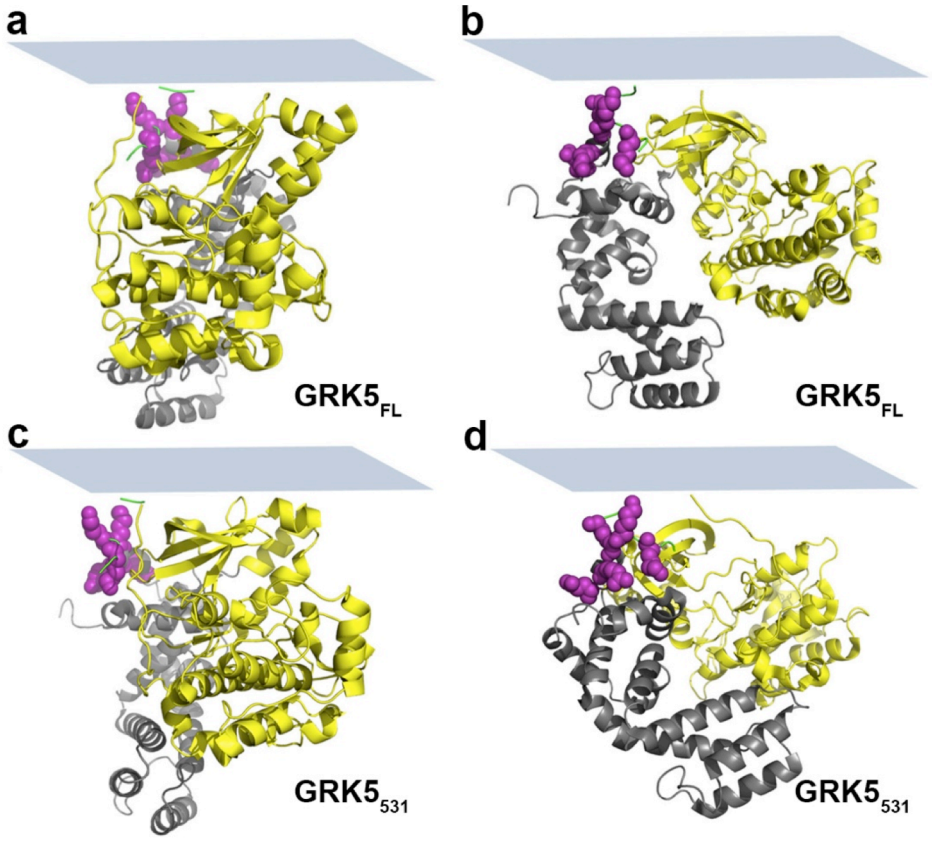

Figure 61. 2ACX model of GRK6 depicting the GRK5 orientation on membrane surface. Two membrane orientations of GRK5FL are shown: **(a)** twist=70°, tilt=2° and **(b)** twist=340°, tilt=10°. Two possible membrane orientations of GRK5531 are similar to that of $GRK5_{FL}$: **(c)** twist=40°, tilt=10° and **(d)** twist=300°, tilt=26°. Modified from (P. Yang et al., 2013).

A.3 Conclusions

The preliminary data of our investigations suggest that GRK5 bind CaM at 1:1 ratio, despite the presence of two CaM-binding sites. When individual peptides were tested for Ca^{2+}/CaM binding affinities in FCPIA experiments, only $GRK5_{20-38}$ bound CaM with high affinity (27 nM). Consistently, Ca^{2+}/CaM was only able to extract $GRK5_{2-31}$ peptide from the lipid bilayers when investigated using ATR-FTIR technique. However, FCPIA experiments performed on the longer GRK5 constructs were somewhat conflicting. Therein the C-terminal deletion ($GRK5_{531}$) and the mutation of the N-terminal CaM-binding site ($GRK5_{NT}$) both led to a decrease in CaM binding affinities (334 and 110 nM for $GRK5_{531}$ and $GRK5_{NT}$, respectively). The truncated GRK5 constructs represent more physiological CaM substrate, compare to peptides. Thus, this data suggests the possibility that N- and C-termini might be spatially close and that somehow both participate in binding of a single CaM molecule.

Mutations, designed to abolish the potential interaction of αCT with the RH domain and the kinase large lobe failed to have any effect on ROS phosphorylation by GRK5, also supporting the hypothesis that its αCT is in a position different from the one observed in GRK6 crystal structure (Boguth *et al.*, 2010).

Finally, our preliminary data with GRK5 FRET sensors, $GRK5_{561}N_{FLASH}$-CFP and $GRK5_{561}67_{FLASH}$-CFP, indicated that αCT is located in the proximity of the RH domain but only in the low ionic strength conditions. This interaction also appeared to be destabilized by the addition of ROS.

Our laboratory has recently solved the crystal structure of GRK5 bound to an inhibitor (Homan KT, Waldschmidt H, Cannavo A, Koch WJ, Tesmer JJG, in preparation). Although the C-terminus of GRK5 was not fully resolved, it appeared that the last visible amino acids of the C-terminus, 530-541 packs close to the N-terminal PIP_2 binding site.

Thus on the basis of all of these observations, our preliminary hypothesis is that the mobile C-terminus of GRK5 adopts multiple conformations. When the kinase is inactive the C-terminus might stabilize GRK5 by interacting with RH domain and the kinase large lobe. When the kinase gets activated, for example when GPCRs are

present, the C-terminus moves to a position close to the N-terminal PIP_2 binding site, so its own phospholipid binding interface at amino acids 552-562 would become accessible for membrane binding. Because both N- and C–terminal CaM binding site would then be located in the proximity of each other, only one CaM molecule would be able to bind due to the steric occlusion of the second site or due to simultaneous binding at both sites.

References

Abe, A., & Shayman, J. A. (1998). Purification and characterization of 1-O-acylceramide synthase, a novel phospholipase A2 with transacylase activity., *J. Biol. Chem. 273*(14), 8467–8474.

Abe, A., & Shayman, J. A. (2009). The role of negatively charged lipids in lysosomal phospholipase A2 function. *J. Lipid Res.*, *50*(10), 2027–2035.

Abe, A., Hiraoka, M., & Shayman, J. A. (2006). Positional specificity of lysosomal phospholipase A2. *J. Lipid Res.*, *47*(10), 2268–2279.

Abe, A., Hiraoka, M., & Shayman, J. A. (2007a). A role for lysosomal phospholipase A2 in drug induced phospholipidosis. *Drug Metab. Lett.*, *1*(1), 49–53.

Abe, A., Hiraoka, M., & Shayman, J. A. (2007b). The acylation of lipophilic alcohols by lysosomal phospholipase A2. *J. Lipid Res.*, *48*(10), 2255–2263.

Abe, A., Hiraoka, M., Wild, S., Wilcoxen, S. E., Paine, R., & Shayman, J. A. (2004a). Lysosomal phospholipase A2 is selectively expressed in alveolar macrophages. *J. Biol. Chem.*, *279*(41), 42605–42611.

Abe, A., Kelly, R., & Shayman, J. A. (2010). The measurement of lysosomal phospholipase A2 activity in plasma. *J. Lipid Res.*, *51*(8), 2464–2470.

Abe, A., Kelly, R., Kollmeyer, J., Hiraoka, M., Lu, Y., & Shayman, J. A. (2008). The secretion and uptake of lysosomal phospholipase A2 by alveolar macrophages. *J. Immunol.*, *181*(11), 7873–7881.

Abe, A., Poucher, H. K., Hiraoka, M., & Shayman, J. A. (2004b). Induction of lysosomal phospholipase A2 through the retinoid X receptor in THP-1 cells. *J. Lipid Res.*, *45*(4), 667–673.

Abe, A., Shayman, J. A., & Radin, N. S. (1996). A novel enzyme that catalyzes the esterification of N-acetylsphingosine. Metabolism of C2-ceramides. *J. Biol. Chem.*, *271*(24), 14383–14389.

Adams, P. D., Afonine, P. V., Bunkóczi, G., Chen, V. B., Davis, I. W., Echols, N., et al. (2010). PHENIX: a comprehensive Python-based system for macromolecular structure solution. *Acta Crystallogr. D 66*(Pt 2), 213–221.

Adimoolam, S., Jin, L., Grabbe, E., Shieh, J. J., & Jonas, A. (1998). Structural and functional properties of two mutants of lecithin-cholesterol acyltransferase (T123I and N228K). *J. Biol. Chem.*, *273*(49), 32561–32567.

Agassandian, M., & Mallampalli, R. K. (2013). Surfactant phospholipid metabolism. *Biochim. Biophys. Acta*, *1831*(3), 612–625.

Aranda, P., Valdivielso, P., Pisciotta, L., Garcia, I., Garcã A-Arias, C., Bertolini, S., et al. (2008). Therapeutic management of a new case of LCAT deficiency with a multifactorial long-term approach based on high doses of angiotensin II receptor blockers (ARBs). *Clinical Nephrology*, *69*(3), 213–218.

Arencibia, J. M., Pastor-Flores, D., Bauer, A. F., Schulze, J. O., & Biondi, R. M. (2013). AGC protein kinases: From structural mechanism of regulation to allosteric drug

development for the treatment of human diseases. *BBA - Proteins and Proteomics*, *1834*(7), 1302–1321.

Argyropoulos, G., Jenkins, A., Klein, R. L., Lyons, T., Wagenhorst, B., St Armand, J., et al. (1998). Transmission of two novel mutations in a pedigree with familial lecithin:cholesterol acyltransferase deficiency: structure-function relationships and studies in a compound heterozygous proband. *J. Lipid Res.*, *39*(9), 1870–1876.

Arpigny, J. L., & Jaeger, K. E. (1999). Bacterial lipolytic enzymes: classification and properties. *Biochem. J.*, *343*, 177–183.

Auge, N., Nègre-Salvayre, A., Salvayre, R., & Levade, T. (2000). Sphingomyelin metabolites in vascular cell signaling and atherogenesis. *Prog. Lipid Res.*, *39*(3), 207–229.

Barton, W. A., Tzvetkova-Robev, D., Erdjument-Bromage, H., Tempst, P., & Nikolov, D. B. (2006). Highly efficient selenomethionine labeling of recombinant proteins produced in mammalian cells. *Protein Sci.*, *15*(8), 2008–2013.

Blanco-Vaca, F., Qu, S. J., Fiol, C., Fan, H. Z., Pao, Q., Marzal-Casacuberta, A., et al. (1997). Molecular basis of fish-eye disease in a patient from Spain. Characterization of a novel mutation in the LCAT gene and lipid analysis of the cornea. *Arterioscl. Throm. Vas.*, *17*(7), 1382–1391.

Boguth, C. A., Singh, P., Huang, C.-C., & Tesmer, J. J. G. (2010). Molecular basis for activation of G protein-coupled receptor kinases. *EMBO J.*, *29*(19), 3249–3259.

Bolin, D. J., & Jonas, A. (1994). Binding of lecithin: cholesterol acyltransferase to reconstituted high density lipoproteins is affected by their lipid but not apolipoprotein composition. *J. Biol. Chem.*, *269*(10), 7429–7434.

Bolin, D. J., & Jonas, A. (1996). Sphingomyelin inhibits the lecithin-cholesterol acyltransferase reaction with reconstituted high density lipoproteins by decreasing enzyme binding. *J. Biol. Chem.*, *271*(32), 19152–8.

Bonelli, F. S., & Jonas, A. (1989). Reaction of lecithin cholesterol acyltransferase with water-soluble substrates. *J. Biol. Chem., 264(25),* 14723-14728.

Bonelli, F. S., & Jonas, A. (1993). Reaction of lecithin: cholesterol acyltransferase with a water soluble substrate: effects of surfactants. *Biochim. Biophys. Acta*, *1166*(1), 92–98.

Boone, T., Meininger, D. P., Schwarz, M., & Shan, B. (2012). Modified lecithin-cholesterol acyltransferase enzymes. (Amgen, Inc). US Patent Office.

Boughton, A. P., Yang, P., & Tesmer, V. M. (2011). Heterotrimeric G protein $\beta_1\gamma_2$ subunits change orientation upon complex formation with G protein-coupled receptor kinase 2 (GRK2) on a model membrane. *P. Natl. Acad. Sci. USA, 108(37),* E667-E673

Calabresi, L., & Francheschini, G. (2010). Genetic LCAT deficiency: molecular diagnosis, plasma lipids, and atherosclerosis. *High Density Lipoproteins*, 89–93.

Calabresi, L., Baldassarre, D., Castelnuovo, S., Conca, P., Bocchi, L., Candini, C., et al. (2009). Functional lecithin: cholesterol acyltransferase is not required for efficient atheroprotection in humans. *Circulation*, *120*(7), 628–635.

Calabresi, L., Pisciotta, L., Costantin, A., Frigerio, I., Eberini, I., Alessandrini, P., et al. (2005). The molecular basis of lecithin:cholesterol acyltransferase deficiency syndromes: a comprehensive study of molecular and biochemical findings in 13 unrelated Italian families. *Arterioscl. Throm. Vas.*, *25*(9), 1972–1978.

Calabresi, L., Simonelli, S., Gomaraschi, M., & Franceschini, G. (2012). Genetic lecithin:cholesterol acyltransferase deficiency and cardiovascular disease. *Atherosclerosis*, *222*(2), 299–306.

Canaan, S., Roussel, A., Verger, R., & Cambillau, C. (1999). Gastric lipase: crystal structure and activity. *Biochim. Biophys. Acta*, *1441*(2-3), 197–204.

Chang, S., McKinsey, T. A., Zhang, C. L., Richardson, J. A., Hill, J. A., & Olson, E. N. (2004). Histone Deacetylases 5 and 9 Govern Responsiveness of the Heart to a Subset of Stress Signals and Play Redundant Roles in Heart Development. *Mol. Cell. Biol.*, *24*(19), 8467–8476.

Chang, V. T., Crispin, M., Aricescu, A. R., Harvey, D. J., Nettleship, J. E., Fennelly, J. A., et al. (2007). Glycoprotein Structural Genomics: Solving the Glycosylation Problem. *Structure*, *15*(3), 267–273.

Charlton-Menys, V., Pisciotta, L., Durrington, P. N., Neary, R., Short, C. D., Calabresi, L., et al. (2007). Molecular characterization of two patients with severe LCAT deficiency. *Nephrol. Dial. Transpl.*, *22*(8), 2379–2382.

Chen, C. K., Zhang, K., Church-Kopish, J., Huang, W., Zhang, H., Chen, Y. J., et al. (2001a). Characterization of human GRK7 as a potential cone opsin kinase. *Mol. Vis.*, *7*, 305–313.

Chen, E. P., Bittner, H. B., Akhter, S. A., Koch, W. J., & Davis, R. D. (2001b). Myocardial function in hearts with transgenic overexpression of the G protein-coupled receptor kinase 5. *Ann. Thorac. Surg.*, *71*(4), 1320–1324.

Chisholm, J. W., Gebre, A. K., & Parks, J. S. (1999). Characterization of C-terminal histidine-tagged human recombinant lecithin:cholesterol acyltransferase. *J. Lipid Res.*, *40*(8), 1512–1519.

Chuang, T. T., Paolucci, L., & De Blasi, A. (1996). Inhibition of G Protein-coupled Receptor Kinase Subtypes by Ca^{2+}/Calmodulin. *J. Biol. Chem.*, *271*(45), 28691–28696.

Cohen, J. C., Kiss, R. S., Pertsemlidis, A., Marcel, Y. L., McPherson, R., & Hobbs, H. H. (2004). Multiple rare alleles contribute to low plasma levels of HDL cholesterol. *Science*, *305*(5685), 869–872.

Collet, X., & Fielding, C. J. (1991). Effects of inhibitors of N-linked oligosaccharide processing on the secretion, stability, and activity of lecithin:cholesterol acyltransferase. *Biochemistry*, *30*(13), 3228–3234.

Contacos, C., Sullivan, D. R., Rye, K. A., Funke, H., & Assmann, G. (1996). A new molecular defect in the lecithin: cholesterol acyltransferase (LCAT) gene associated with fish eye disease. *J. Lipid Res.*, *37*(1), 35–44.

Dennis, E. A., Cao, J., Hsu, Y.-H., Magrioti, V., & Kokotos, G. (2011). Phospholipase A 2Enzymes: Physical Structure, Biological Function, Disease Implication, Chemical Inhibition, and Therapeutic Intervention. *Chem. Rev.*, *111*(10), 6130–6185.

Ding, B., Glukhova, A., Sobczyk-Kojiro, K., Mosberg, H. I., Tesmer, J. J. G., & Chen, Z. (2014). Unveiling the membrane-binding properties of N-terminal and C-terminal regions of G protein-coupled receptor kinase 5 by combined optical spectroscopies. *Langmuir*, *30*(3), 823–831.

Dranoff, G., Crawford, A. D., Sadelain, M., & Ream, B. (1994). Involvement of granulocyte-macrophage colony-stimulating factor in pulmonary homeostasis. *Science, 264,* 713-716

Egloff, M. P., Marguet, F., Buono, G., & Verger, R. (1995). The 2.46. Å Resolution Structure of the Pancreatic Lipase-Colipase Complex Inhibited by a C11 Alkyl Phosphonate. *Biochemistry, 34,* 2751-2762

Elbein, A. D. (1987). Inhibitors of the biosynthesis and processing of N-linked oligosaccharide chains. *Annu. Rev. Biochem, 56,* 497-534.

Emsley, P., Lohkamp, B., Scott, W. G., & Cowtan, K. (2010). Features and development of Coot. *Acta Crystallogr. D, 66*, 486–501.

Evans, P. (2006). Scaling and assessment of data quality. *Acta Crystallogr. D*, *62*, 72–82.

Ferguson, S. S. (2001). Evolving concepts in G protein-coupled receptor endocytosis: the role in receptor desensitization and signaling. *Pharmacol. Rev.*, *53*(1), 1–24.

Fielding, C. J., Shore, V. G., & Fielding, P. E. (1972). A protein cofactor of lecithin:cholesterol acyltransferase. *Biochem. Bioph. Res. Co.*, *46*(4), 1493–1498.

Francone, O. L., & Fielding, C. J. (1991a). Effects of site-directed mutagenesis at residues cysteine-31 and cysteine-184 on lecithin-cholesterol acyltransferase activity. *P. Natl. Acad. Sci. USA*, *88*(5), 1716–1720.

Francone, O. L., & Fielding, C. J. (1991b). Structure-function relationships in human lecithin: cholesterol acyltransferase. Site-directed mutagenesis at serine residues 181 and 216. *Biochemistry, 30,* 10074-10077

Francone, O. L., Evangelista, L., & Fielding, C. J. (1993). Lecithin-cholesterol acyltransferase: effects of mutagenesis at N-linked oligosaccharide attachment sites on acyl acceptor specificity. *Biochim. Biophys. Acta, 1166,* 301-304

Francone, O. L., Evangelista, L., & Fielding, C. J. (1996). Effects of carboxy-terminal truncation on human lecithin:cholesterol acyltransferase activity. *J. Lipid Res.*, *37*(7), 1609–15.

Frascà, G. M., Soverini, L., Tampieri, E., Franceschini, G., Calabresi, L., Pisciotta, L., et al. (2004). A 33-year-old man with nephrotic syndrome and lecithin-cholesterol acyltransferase (LCAT) deficiency. Description of two new mutations in the LCAT gene. *Nephrol. Dial. Transpl.*, *19*(6), 1622–1624.

Fredericks, Z. L., Pitcher, J. A., & Lefkowitz, R. J. (1996). Identification of the G protein-coupled receptor kinase phosphorylation sites in the human beta2-adrenergic receptor. *J. Biol. Chem.*, *271*(23), 13796–13803.

Freedman, N. J., Liggett, S. B., Drachman, D. E., Pei, G., Caron, M. G., & Lefkowitz, R. J. (1995). Phosphorylation and desensitization of the human β_1-adrenergic receptor. Involvement of G protein-coupled receptor kinases and cAMP-dependent protein kinase. *J. Biol. Chem.*, *270*(30), 17953–17961.

Funke, H., Eckardstein, von, A., Pritchard, P. H., Albers, J. J., Kastelein, J. J., Droste, C., & Assmann, G. (1991). A molecular defect causing fish eye disease: an amino acid exchange in lecithin-cholesterol acyltransferase (LCAT) leads to the selective loss of alpha-LCAT activity. *P. Natl. Acad. Sci. USA*, *88*(11), 4855–4859.

Funke, H., Eckardstein, von, A., Pritchard, P. H., Hornby, A. E., Wiebusch, H., Motti, C., et al. (1993). Genetic and phenotypic heterogeneity in familial lecithin: cholesterol acyltransferase (LCAT) deficiency. *J. Clin. Invest.*, *91*(2), 677–683.

Gainetdinov, R. R., Bohn, L. M., Walker, J. K., Laporte, S. A., Macrae, A. D., Caron, M. G., et al. (1999). Muscarinic supersensitivity and impaired receptor desensitization in G protein-coupled receptor kinase 5-deficient mice. *Neuron*, *24*(4), 1029–1036.

Glomset, J. A., Janssen, E. T., Kennedy, R., & Dobbins, J. (1966). Role of plasma lecithin:cholesterol acyltransferase in the metabolism of high density lipoproteins. *J. Lipid Res.*, *7*(5), 638–648.

Gold, J. I., Martini, J. S., Hullmann, J., Gao, E., Chuprun, J. K., Lee, L., et al. (2013). Nuclear translocation of cardiac G protein-Coupled Receptor kinase 5 downstream of select Gq-activating hypertrophic ligands is a calmodulin-dependent process. *PloS One*, *8*(3), e57324.

Goldschmidt, L., Cooper, D. R., Derewenda, Z. S., & Eisenberg, D. (2007). Toward rational protein crystallization: A Web server for the design of crystallizable protein variants. *Protein Sci.*, *16*(8), 1569–1576.

Gotoda, T., Yamada, N., Murase, T., Sakuma, M., Murayama, N., Shimano, H., et al. (1991). Differential phenotypic expression by three mutant alleles in familial lecithin:cholesterol acyltransferase deficiency. *The Lancet*, *338*(8770), 778–781.

Goyal, J., Wang, K., Liu, M., & Subbaiah, P. V. (1997). Novel Function of Lecithin-Cholesterol Acyltransferase:Hydrolysis of Oxidized Polar Phospholipids Generated During Lipoprotein Oxidation. *J. Biol. Chem., 272 (26),* 16231-16239

Griffin, B. A., Adams, S. R., Jones, J., & Tsien, R. Y. (2000). Fluorescent labeling of recombinant proteins in living cells with FlAsH. *Method. Enzymol.*, *327*, 565–78.

Grochulski, P., Bouthillier, F., Kazlauskas, R. J., Serreqi, A. N., Schrag, J. D., Ziomek, E., & Cygler, M. (1994). Analogs of reaction intermediates identify a unique substrate binding site in Candida rugosa lipase. *Biochemistry*, *33*(12), 3494–3500.

Grove, D., & Pownall, H. J. (1991). Comparative specificity of plasma lecithin:cholesterol acyltransferase from ten animal species. *Lipids*, *26*(6), 416–20.

Grueninger-Leitch, F., D'Arcy, A., D'Arcy, B., & Chène, C. (1996). Deglycosylation of proteins for crystallization using recombinant fusion protein glycosidases. *Protein Sci.*, *5*(12), 2617–2622.

Hanyaloglu, A. C., & Zastrow, M. V. (2008). Regulation of GPCRs by Endocytic Membrane Trafficking and Its Potential Implications. *Annu. Rev. Pharmacol.*, *48*(1), 537–568.

Heath, M. F., Costa-Jussà, F. R., Jacobs, J. M., & Jacobson, W. (1985). The induction of pulmonary phospholipidosis and the inhibition of lysosomal phospholipases by amiodarone. *Brit. J. Exp. Pathol.*, *66*(4), 391–397.

Hill, J. S., O, K., Wang, X., & Pritchard, P. H. (1993a). Lecithin:cholesterol acyltransferase deficiency: identification of a causative gene mutation and a co-inherited protein polymorphism. *Biochim. Biophys. Acta*, *1181*(3), 321–323.

Hill, J. S., Wang, X., & Pritchard, P. H. (1993b). Recombinant lecithin: cholesterol acyltransferase containing a Thr123 -> Ile mutation esterifies cholesterol in low density lipoprotein but not in high density lipoprotein. *J. Lipid Res., 34,* 81-88

Hiraoka, M., Abe, A., & Shayman, J. A. (2002). Cloning and characterization of a lysosomal phospholipase A2, 1-O-acylceramide synthase. *J. Biol. Chem.*, *277*(12), 10090–10099.

Hiraoka, M., Abe, A., & Shayman, J. A. (2005). Structure and function of lysosomal phospholipase A2: identification of the catalytic triad and the role of cysteine residues. *J. Lipid Res.*, *46*(11), 2441–2447.

Hiraoka, M., Abe, A., Lu, Y., Yang, K., Han, X., Gross, R. W., & Shayman, J. A. (2006). Lysosomal phospholipase A2 and phospholipidosis. *Mol. Cell. Biol.*, *26*(16), 6139–

6148.
Hiraoka, M., Okamoto, K., Ohguro, H., & Abe, A. (2013). Role of N-glycosylation of human lysosomal phospholipase A2 for the formation of catalytically active enzyme. *J. Lipid Res.*, *54*(11), 3098–3105.
Hisatomi, O., Matsuda, S., Satoh, T., Kotaka, S., Imanishi, Y., & Tokunaga, F. (1998). A novel subtype of G-protein-coupled receptor kinase, GRK7, in teleost cone photoreceptors. *FEBS Lett.*, *424*(3), 159–164.
Hoang, A., Huang, W., Sasaki, J., & Sviridov, D. (2003). Natural mutations of apolipoprotein AI impairing activation of lecithin: cholesterol acyltransferase. *Biochim. Biophys. Acta, 1631,* 72-76
Holleboom, A. G., Kuivenhoven, J. A., Peelman, F., Schimmel, A. W., Peter, J., Defesche, J. C., et al. (2011a). High prevalence of mutations in LCAT in patients with low HDL cholesterol levels in The Netherlands: identification and characterization of eight novel mutations. *Hum. Mutat.*, *32*(11), 1290–1298.
Holleboom, A. G., Kuivenhoven, J. A., van Olden, C. C., Peter, J., Schimmel, A. W., Levels, J. H., et al. (2011b). Proteinuria in early childhood due to familial LCAT deficiency caused by loss of a disulfide bond in lecithin:cholesterol acyl transferase. *Atherosclerosis*, *216*(1), 161–165.
Hörl, G., Kroisel, P. M., Wagner, E., Tiran, B., Petek, E., & Steyrer, E. (2006). Compound heterozygosity (G71R/R140H) in the lecithin:cholesterol acyltransferase (LCAT) gene results in an intermediate phenotype between LCAT-deficiency and fish-eye disease. *Atherosclerosis*, *187*(1), 101–109.
Hu, L. A., Chen, W., Premont, R. T., Cong, M., & Lefkowitz, R. J. (2002). G protein-coupled receptor kinase 5 regulates beta 1-adrenergic receptor association with PSD-95. *J. Biol. Chem.*, *277*(2), 1607–1613.
Ikegami, M., Ueda, T., Hull, W., Whitsett, J. A., Mulligan, R. C., Dranoff, G., & Jobe, A. H. (1996). Surfactant metabolism in transgenic mice after granulocyte macrophage-colony stimulating factor ablation. *Am. J. Physiol*, *270*(4 Pt 1), L650–8.
Inglese, J., Koch, W. J., Caron, M. G., & Lefkowitz, R. J. (1992). Isoprenylation in regulation of signal transduction by G-protein-coupled receptor kinases. *Nature*, *359*(6391), 147–150.
Itabe, H., Hosoya, R., Karasawa, K., Jimi, S., Saku, K., Takebayashi, S., et al. (1999). Metabolism of oxidized phosphatidylcholines formed in oxidized low density lipoprotein by lecithin-cholesterol acyltransferase. *J. Biochem.-Tokyo*, *126*(1), 153–161.
Jaber, M., Koch, W. J., Rockman, H., Smith, B., Bond, R. A., Sulik, K. K., et al. (1996). Essential role of beta-adrenergic receptor kinase 1 in cardiac development and function. *P. Natl. Acad. Sci. USA*, *93*(23), 12974–12979.
Jaeger, K. E., Ransac, S., Dijkstra, B. W., Colson, C., van Heuvel, M., & Misset, O. (1994). Bacterial lipases. *FEMS Microbiology Reviews*, *15*(1), 29–63.
Jalili, T., Takeishi, Y., & Walsh, R. A. (1999). Signal transduction during cardiac hypertrophy: the role of Gαq, PLC βI, and PKC. *Cardiovasc. Res.*, *44*(1), 5–9.
Jauhiainen, M., & Dolphin, P. J. (1986). Human plasma lecithin-cholesterol acyltransferase. An elucidation of the catalytic mechanism. *J. Biol. Chem.*, *261*(15), 7032–7043.
Jauhiainen, M., Stevenson, K. J., & Dolphin, P. J. (1988). Human plasma lecithin-

cholesterol acyltransferase. The vicinal nature of cysteine 31 and cysteine 184 in the catalytic site. *J. Biol. Chem.*, *263*(14), 6525–6533.

Johnson, L. R., Scott, M. G. H., & Pitcher, J. A. (2004). G Protein-Coupled Receptor Kinase 5 Contains a DNA-Binding Nuclear Localization Sequence. *Mol. Cell. Biol.*, *24*(23), 10169–10179.

Jonas, A., Daehler, J. L., & Wilson, E. R. (1986). Anion effects on the reaction of lecithin-cholesterol acyltransferase with discoidal complexes of phosphatidylcholines-apolipoprotein A-I -cholesterol. *Biochim. Biophys. Acta*, *876*(3), 474–485.

Jonas, A., & Phillips, M. C. (2008). Lipoprotein structure. In D. E. Vance & J. E. Vance, *Biochemistry of Lipids, Lipoproteins and Membranes* (5 ed., pp. 485–506). Elsevier.

Jonas, A., Sweeny, S. A., & Herbert, P. N. (1984). Discoidal complexes of A and C apolipoproteins with lipids and their reactions with lecithin: cholesterol acyltransferase. *J. Biol. Chem.*, *259*(10), 6369–6375.

Kabsch, W. (2010). XDS. *Acta Crystallogr. D*, *66*, 125–132.

Kim, D. E., Chivian, D., & Baker, D. (2004). Protein structure prediction and analysis using the Robetta server. *Nucleic Acids Res.*, *32*, W526–W531.

Kitabatake, K., Piran, U., Kamio, Y., Doi, Y., & Nishida, T. (1979). Purification of human plasma lecithin:cholesterol acyltransferase and its specificity towards the acyl acceptor. *Biochim. Biophys. Acta*, *573*(1), 145–154.

Klein, H. G., Duverger, N., Albers, J. J., Marcovina, S., Brewer, H. B., & Santamarina-Fojo, S. (1995). In vitro expression of structural defects in the lecithin-cholesterol acyltransferase gene. *J. Biol. Chem.*, *270*(16), 9443–9447.

Klein, H. G., Lohse, P., Duverger, N., Albers, J. J., Rader, D. J., Zech, L. A., et al. (1993). Two different allelic mutations in the lecithin:cholesterol acyltransferase (LCAT) gene resulting in classic LCAT deficiency: LCAT (tyr83->stop) and LCAT (tyr156->asn). *J. Lipid Res.*, *34*(1), 49–58.

Klein, H. G., Lohse, P., Pritchard, P. H., Bojanovski, D., Schmidt, H., & Brewer, H. B., Jr. (1992). Two different allelic mutations in the lecithin-cholesterol acyltransferase gene associated with the fish eye syndrome. Lecithin-cholesterol acyltransferase (Thr123Ile) and lecithin-cholesterol acyltransferase (Thr347-Met). *J. Clin. Invest.*, *89*(2), 499–506.

Korbel, D. S., Schneider, B. E., & Schaible, U. E. (2008). Innate immunity in tuberculosis: myths and truth. *Microbes and Infect.*, *10*(9), 995–1004.

Kosman, J., & Jonas, A. (2001). Deletion of specific glycan chains affects differentially the stability, local structures, and activity of lecithin-cholesterol acyltransferase. *J. Biol. Chem.*, *276*(40), 37230–37236.

Krissinel, E., & Henrick, K. (2007). Inference of Macromolecular Assemblies from Crystalline State. *J. Mol. Biol.*, *372*(3), 774–797.

Kuivenhoven, J. A., Stalenhoef, A. F. H., Hill, J. S., Demacker, P. N. M., Errami, A., Kastelein, J. J. P., & Pritchard, P. H. (1996). Two Novel Molecular Defects in the LCAT Gene Are Associated With Fish Eye Disease. *Arterioscl. Throm. Vas.*, *16*(2), 294–303.

Kuivenhoven, J. A., van Voorst tot Voorst, E. J., Wiebusch, H., Marcovina, S. M., Funke, H., Assmann, G., et al. (1995). A unique genetic and biochemical presentation of fish-eye disease. *J. Clin. Invest.*, *96*(6), 2783–2791.

Kunapuli, P., Gurevich, V. V., & Benovic, J. L. (1994a). Phospholipid-stimulated autophosphorylation activates the G protein-coupled receptor kinase GRK5. *J. Biol. Chem.*, *269*(14), 10209–10212.

Kunapuli, P., Onorato, J. J., Hosey, M. M., & Benovic, J. L. (1994b). Expression, purification, and characterization of the G protein-coupled receptor kinase GRK5. *J. Biol. Chem.*, *269*(2), 1099–105.

Kunnen, S., & Van Eck, M. (2012). Lecithin:cholesterol acyltransferase: old friend or foe in atherosclerosis? *J. Lipid Res.*, *53*(9), 1783–1799.

Kwan, E. M., Boraston, A. B., McLean, B. W., Kilburn, D. G., & Warren, R. A. J. (2005). N-Glycosidase-carbohydrate-binding module fusion proteins as immobilized enzymes for protein deglycosylation. *Protein Eng. Des. Sel.*, *18*(10), 497–501.

Lebedev, A. A., Young, P., Isupov, M. N., Moroz, O. V., Vagin, A. A., & Murshudov, G. N. (2012). JLigand: a graphical tool for the CCP4 template-restraint library. *Acta Crystallogr. D*, *68*(Pt 4), 431–440.

Lee, T. C., Malone, B., Blank, M. L., Fitzgerald, V., & Snyder, F. (1990). Regulation of the synthesis of platelet-activating factor and its inactive storage precursor (1-alkyl-2-acyl-sn-glycero-3-phosphocholine) from 1-alkyl-2-acetyl-sn-glycerol by rabbit platelets. *J. Biol. Chem.*, *265*(16), 9181–9187.

Lee, T., Ou, M., Shinozaki, K., & Malone, B. (1996). Biosynthesis of N-acetylsphingosine by platelet-activating factor: sphingosine CoA-independent transacetylase in HL-60 cells. *J. Biol. Chem.*, *271*(1), 209–217.

Lee, Y. P., Adimoolam, S., Liu, M., Subbaiah, P. V., Glenn, K., & Jonas, A. (1997). Analysis of human lecithin-cholesterol acyltransferase activity by carboxyl-terminal truncation. *Biochim. Biophys. Acta*, *1344*(3), 250–261.

Levay, K., Satpaev, D. K., Pronin, A. N., Benovic, J. L., & Slepak, V. Z. (1998). Localization of the sites for Ca^{2+}-binding proteins on G protein-coupled receptor kinases. *Biochemistry*, *37*(39), 13650–13659.

Li, H., Das, A., Sibhatu, H., Jamal, J., Sligar, S. G., & Poulos, T. L. (2008). Exploring the Electron Transfer Properties of Neuronal Nitric-oxide Synthase by Reversal of the FMN Redox Potential. *J. Biol. Chem.*, *283*(50), 34762–34772.

Liggett, S. B., Ostrowski, J., Chesnut, L. C., Kurose, H., Raymond, J. R., Caron, M. G., & Lefkowitz, R. J. (1992). Sites in the third intracellular loop of the alpha 2A-adrenergic receptor confer short term agonist-promoted desensitization. Evidence for a receptor kinase-mediated mechanism. *The J. Biol. Chem.*, *267*(7), 4740–4746.

Lin, D. S., Steiner, R. D., Merkens, L. S., Pappu, A. S., & Connor, W. E. (2010). The effects of sterol structure upon sterol esterification. *Atherosclerosis*, *208*(1), 155–160.

Liu, M., & Subbaiah, P. V. (1993). Activation of plasma lysolecithin acyltransferase reaction by apolipoproteins A-I, C-I and E. *Biochim. Biophys. Acta*, *1168*(2), 144–152.

Liu, M., & Subbaiah, P. V. (1994). Hydrolysis and transesterification of platelet-activating factor by lecithin-cholesterol acyltransferase. *P. Natl. Acad. Sci. USA*, *91*(13), 6035–6039.

Liu, M., Subramanian, V. S., & Subbaiah, P. V. (1998). Modulation of the positional specificity of lecithin-cholesterol acyltransferase by the acyl group composition of its phosphatidylcholine substrate: role of the sn-1-acyl group. *Biochemistry*, *37*(39),

13626–13633.
Lodowski, D. T., Tesmer, V. M., Benovic, J. L., & Tesmer, J. J. G. (2006). The structure of G protein-coupled receptor kinase (GRK)-6 defines a second lineage of GRKs. *J. Biol. Chem.*, *281*(24), 16785–16793.
Madhusudan, Akamine, P., Xuong, N.-H., & Taylor, S. S. (2002). Crystal structure of a transition state mimic of the catalytic subunit of cAMP-dependent protein kinase. *Nat. Struct. Biol.*, *9*(4), 273–277.
Maiolino, G., Rossitto, G., Caielli, P., Bisogni, V., Rossi, G. P., & Calò, L. A. (2013). The role of oxidized low-density lipoproteins in atherosclerosis: the myths and the facts. *Mediat. Inflamm.*, *2013*, 714653.
Maley, F., Trimble, R. B., Tarentino, A. L., & Plummer, T. H. (1989). Characterization of glycoproteins and their associated oligosaccharides through the use of endoglycosidases. *Anal. Biochem.*, *180*(2), 195–204.
Mallat, Z., & Tedgui, A. (2001). Current perspective on the role of apoptosis in atherothrombotic disease. *Circ. Res.*, *88*(10), 998–1003.
Malur, A., Kavuru, M. S., Marshall, I., Barna, B. P., Huizar, I., Karnekar, R., & Thomassen, M. J. (2012). Rituximab therapy in pulmonary alveolar proteinosis improves alveolar macrophage lipid homeostasis., *Respir. Res., 13(46),* 1-7
Martinez, C., Nicolas, A., van Tilbeurgh, H., Egloff, M. P., Cudrey, C., Verger, R., & Cambillau, C. (1994). Cutinase, a lipolytic enzyme with a preformed oxyanion hole. *Biochemistry*, *33*(1), 83–89.
Martini, J. S., Raake, P., Vinge, L. E., DeGeorge, B. R., Chuprun, J. K., Harris, D. M., et al. (2008). Uncovering G protein-coupled receptor kinase-5 as a histone deacetylase kinase in the nucleus of cardiomyocytes. *P. Natl. Acad. Sci. USA*, *105*(34), 12457–12462.
McCoy, A. J., Grosse-Kunstleve, R. W., Adams, P. D., Winn, M. D., Storoni, L. C., & Read, R. J. (2007). Phaser crystallographic software. *J. Appl. Crystallogr.*, *40*(Pt 4), 658–674.
McKinsey, T. A., Zhang, C. L., Lu, J., & Olson, E. N. (2000). Signal-dependent nuclear export of a histone deacetylase regulates muscle differentiation. *Nature*, *408*(6808), 106–111.
McLean, J. (1992). Molecular defects in the lecithin:cholesterol acyl-transferase gene. In *High Density Lipoproteins and Atherosclerosis III* (N. E. Miller & A. R. Tall, eds.), pp. 59–65, Elsevier, Amsterdam.
Miettinen, H. E., Gylling, H., Tenhunen, J., Virtamo, J., Jauhiainen, M., Huttunen, J. K., et al. (1998). Molecular Genetic Study of Finns With Hypoalphalipoproteinemia and Hyperalphalipoproteinemia : A Novel Gly230Arg Mutation (LCATFin) of Lecithin:Cholesterol Acyltransferase (LCAT) Accounts for 5% of Cases With Very Low Serum HDL Cholesterol Levels. *Arterioscl. Throm. Vas.*, *18*(4), 591–598.
Miettinen, H., Gylling, H., Ulmanen, I., Miettinen, T. A., & Kontula, K. (1995). Two different allelic mutations in a Finnish family with lecithin:cholesterol acyltransferase deficiency. *Arterioscl. Throm. Vas.*, *15*(4), 460–467.
Miled, N., Bussetta, C., De caro, A., Rivière, M., Berti, L., & Canaan, S. (2003). Importance of the lid and cap domains for the catalytic activity of gastric lipases. *Comparative Biochemistry and Physiology Part B: Biochemistry and Molecular Biology*, *136*(1), 131–138.

Miller, K. R., & Parks, J. S. (1997). Influence of vesicle surface composition on the interfacial binding of lecithin: cholesterol acyltransferase and apolipoprotein AI. *J. Lipid Res., 38,* 1094-1102

Miller, K. R., Wang, J., Sorci-Thomas, M., Anderson, R. A., & Parks, J. S. (1996). Glycosylation structure and enzyme activity of lecithin:cholesterol acyltransferase from human plasma, HepG2 cells, and baculoviral and Chinese hamster ovary cell expression systems. *J. Lipid Res.*, *37*(3), 551–561.

Minnich, A., Collet, X., Roghani, A., Cladaras, C., Hamilton, R. L., Fielding, C. J., & Zannis, V. I. (1992). Site-directed mutagenesis and structure-function analysis of the human apolipoprotein AI. Relation between lecithin-cholesterol acyltransferase activation and lipid binding. *J. Biol. Chem.*, *267*(23), 16553–16560.

Moriyama, K., Sasaki, J., Arakawa, F., Takami, N., Maeda, E., Matsunaga, A., et al. (1995). Two novel point mutations in the lecithin:cholesterol acyltransferase (LCAT) gene resulting in LCAT deficiency: LCAT (G873 deletion) and LCAT (Gly344->Ser). *J. Lipid Res.*, *36*(11), 2329–2343.

Murphy, G., Lisnevskaia, L., & Isenberg, D. (2013). Systemic lupus erythematosus and other autoimmune rheumatic diseases: challenges to treatment. *The Lancet, S0140-6736(14),* 60128-8

Murray, K. R., Nair, M. P., Ayyobi, A. F., Hill, J. S., Pritchard, P. H., & Lacko, A. G. (2001). Probing the 121-136 domain of lecithin:cholesterol acyltransferase using antibodies. *Arch. Biochem. Biophys.*, *385*(2), 267–275.

Murshudov, G. N., Skubák, P., Lebedev, A. A., Pannu, N. S., Steiner, R. A., Nicholls, R. A., et al. (2011). REFMAC5 for the refinement of macromolecular crystal structures. *Acta Crystallogr. D*, *67*, 355–367.

Nanjee, M. (2003). A novel LCAT mutation (Phe382→Val) in a kindred with familial LCAT deficiency and defective apolipoprotein B-100. *Atherosclerosis*, *170*(1), 105–113.

Nardini, M., & Dijkstra, B. W. (1999). α/β hydrolase fold enzymes: the family keeps growing. *Curr. Opin. Struc. Biol.*, *9*(6), 732–737.

Nardini, M., Lang, D. A., Liebeton, K., Jaeger, K. E., & Dijkstra, B. W. (2000). Crystal structure of pseudomonas aeruginosa lipase in the open conformation. *J. Biol. Chem.*, *275*(40), 31219–31225.

O, K., Hill, J. S., Wang, X., McLeod, R., & Pritchard, P. H. (1993). Lecithin:cholesterol acyltransferase: role of N-linked glycosylation in enzyme function. *Biochem. J.*, *294 (Pt 3)*, 879–84.

Ollis, D. L., Cheah, E., Cygler, M., & Dijkstra, B. (1992). The α/β hydrolase fold. *Protein Eng.*, *5*(3), 197–211.

Oppermann, M., Freedman, N. J., & Alexander, R. W. (1996). Phosphorylation of the type 1A angiotensin II receptor by G protein-coupled receptor kinases and protein kinase C. *J. Biol. Chem.*, *271*(22), 13266–13272.

Otwinowski, Z., & Minor, W. (1997). Processing of X-ray diffraction data collected in oscillation mode. *Method. Enzymol.*, *276*, 307–326.

Paduraru, C., Bezbradica, J. S., Kunte, A., Kelly, R., Shayman, J. A., Veerapen, N., et al. (2013). Role for lysosomal phospholipase A2 in iNKT cell-mediated CD1d recognition. *P. Natl. Acad. Sci. USA a*, *110*(13), 5097–5102.

Parks, J. S., Huggins, K. W., Gebre, A. K., & Burleson, E. R. (2000).

Phosphatidylcholine fluidity and structure affect lecithin:cholesterol acyltransferase activity. *J. Lipid Res.*, *41*(4), 546–53.

Parks, J. S., Thuren, T. Y., & Schmitt, J. D. (1992). Inhibition of lecithin: cholesterol acyltransferase activity by synthetic phosphatidylcholine species containing eicosapentaenoic acid or docosahexaenoic acid in the *sn-2* position. *J. Lipid Res., 33,* 879-887

Peelman, F., Verschelde, J. L., Vanloo, B., Ampe, C., Labeur, C., Tavernier, J., et al. (1999). Effects of natural mutations in lecithin:cholesterol acyltransferase on the enzyme structure and activity. *J. Lipid Res.*, *40*(1), 59–69.

Peelman, F., Vinaimont, N., Verhee, A., Vanloo, B., Verschelde, J. L., Labeur, C., et al. (1998). A proposed architecture for lecithin cholesterol acyl transferase (LCAT): identification of the catalytic triad and molecular modeling. *Protein Sci.*, *7*(3), 587–99.

Peng, J., & Xu, J. (2011). Raptorx: Exploiting structure information for protein alignment by statistical inference. *Proteins: Struct., Funct., Bioinf.*, *79*(S10), 161–171.

Pettersen, E. F., Goddard, T. D., Huang, C. C., Couch, G. S., Greenblatt, D. M., Meng, E. C., & Ferrin, T. E. (2004). UCSF Chimera - a visualization system for exploratory research and analysis. *J. Comput. Chem.*, *25*(13), 1605–1612.

Piran, U., & Nishida, T. (1979). Utilization of various sterols by lecithin-cholesterol acyltransferase as acyl acceptors. *Lipids*, *14*(5), 478–482.

Pitcher, J. A., Fredericks, Z. L., Stone, W. C., Premont, R. T., Stoffel, R. H., Koch, W. J., & Lefkowitz, R. J. (1996). Phosphatidylinositol 4,5-bisphosphate (PIP2)-enhanced G protein-coupled receptor kinase (GRK) activity. *J. Biol. Chem.*, *271*(40), 24907–24913.

Pitcher, J. A., Freedman, N. J., & Lefkowitz, R. J. (1998). G protein-coupled receptor kinases. *Annu. Rev. Biochem.*, *67*(1), 653–692.

Pitcher, J. A., Inglese, J., Higgins, J. B., Arriza, J. L., Casey, P. J., Kim, C., et al. (1992). Role of beta gamma subunits of G proteins in targeting the beta-adrenergic receptor kinase to membrane-bound receptors. *Science*, *257*(5074), 1264–1267.

Pownall, H. J., Pao, Q., & Massey, J. B. (1985). Acyl chain and headgroup specificity of human plasma lecithin:cholesterol acyltransferase. Separation of matrix and molecular specificities. *J. Biol. Chem.*, *260*(4), 2146–2152.

Premont, R. T., Koch, W. J., Inglese, J., & Lefkowitz, R. J. (1994). Identification, purification, and characterization of GRK5, a member of the family of G protein-coupled receptor kinases. *J. Biol. Chem.*, *269*(9), 6832–6841.

Premont, R. T., Macrae, A. D., Stoffel, R. H., & Chung, N. (1996). Characterization of the G Protein-coupled Receptor Kinase GRK4 Identification Of Four Splice Variants. *J. Biol. Chem.y*, *271*(11), 6403–6410.

Pronin, A. N., & Benovic, J. L. (1997). Regulation of the G Protein-coupled Receptor Kinase GRK5 by Protein Kinase C. *J. Biol. Chem.*, *272*(6), 3806–3812.

Pronin, A. N., Carman, C. V., & Benovic, J. L. (1998). Structure-Function Analysis Of G Protein-Coupled Receptor Kinase-5: Role Of The Carboxyl Terminus In Kinase Regulation. *J. Biol. Chem.*, *273*(47), 31510–31518.

Pronin, A. N., Satpaev, D. K., & Slepak, V. Z. (1997). Regulation of G protein-coupled receptor kinases by calmodulin and localization of the calmodulin binding domain. *J. Biol. Chem.*, *272*(29), 18273–18280.

Qu, S. J., Fan, H. Z., Blanco-Vaca, F., & Pownall, H. J. (1993). Effects of site-directed mutagenesis on the N-glycosylation sites of human lecithin: cholesterol acyltransferase. *Biochemistry*, *32*(34), 8732–8736.

Qu, S. J., Fan, H. Z., Blanco-Vaca, F., & Pownall, H. J. (1994). Effects of site-directed mutagenesis on the serine residues of human lecithin:cholesterol acyltransferase. *Lipids*, *29*(12), 803–9.

Qu, S. J., Fan, H. Z., Blanco-Vaca, F., & Pownall, H. J. (1995). In vitro expression of natural mutants of human lecithin:cholesterol acyltransferase. *J. Lipid Res.*, *36*(5), 967–74.

Rader, D. J., Ikewaki, K., Duverger, N., Schmidt, H., Pritchard, H., Frohlich, J., et al. (1994). Markedly accelerated catabolism of apolipoprotein A-II (ApoA-II) and high density lipoproteins containing ApoA-II in classic lecithin: cholesterol acyltransferase deficiency and fish-eye disease. *J. Clin. Invest.*, *93*(1), 321–330.

Reasor, M. J., & Kacew, S. (2001). Drug-induced phospholipidosis: are there functional consequences? *Exp. Biol. Med.*, *226*(9), 825–830.

Reeves, P. J., Callewaert, N., Contreras, R., & Khorana, H. G. (2002). Structure and function in rhodopsin: high-level expression of rhodopsin with restricted and homogeneous N-glycosylation by a tetracycline-inducible N-acetylglucosaminyltransferase I-negative HEK293S stable mammalian cell line. *P. Natl. Acad. Sci. USA*, *99*(21), 13419–13424.

Reynolds, L. J., Hughes, L. L., Louis, A. I., Kramer, R. M., & Dennis, E. A. (1993). Metal ion and salt effects on the phospholipase A2, lysophospholipase, and transacylase activities of human cytosolic phospholipase A2. *Biochim. Biophys. Acta*, *1167*(3), 272–280.

Ricciotti, E., & FitzGerald, G. A. (2011). Prostaglandins and inflammation. *Arterioscl. Throm. Vas.*, *31*(5), 986–1000.

Rockman, H. A., Choi, D. J., Rahman, N. U., Akhter, S. A., Lefkowitz, R. J., & Koch, W. J. (1996). Receptor-specific in vivo desensitization by the G protein-coupled receptor kinase-5 in transgenic mice. *P. Natl. Acad. Sci. USA*, *93*(18), 9954–9959.

Roman, D. L., Ota, S., & Neubig, R. R. (2009). Polyplexed Flow Cytometry Protein Interaction Assay: A Novel High-Throughput Screening Paradigm for RGS Protein Inhibitors. *J. Biomol. Screen.*, *14*(6), 610–619.

Rosenwald, A. G., & Pagano, R. E. (1994). Effects of the glucosphingolipid synthesis inhibitor, PDMP, on lysosomes in cultured cells. *J. Lipid Res.*, *35*(7), 1232–1240.

Roshan, B., Ganda, O. P., Desilva, R., Ganim, R. B., Ward, E., Haessler, S. D., et al. (2011). Homozygous lecithin:cholesterol acyltransferase (LCAT) deficiency due to a new loss of function mutation and review of the literature. *J. Clin. Lipidol.*, *5*(6), 493–499.

Rosset, J., Wang, J., Wolfe, B. M., Dolphin, P. J., & Hegele, R. A. (2001). Lecithin:cholesterol acyl transferase G30S: association with atherosclerosis, hypoalphalipoproteinemia and reduced in vivo enzyme activity. *Clin. Biochem.*, *34*(5), 381–386.

Roussel, A., Miled, N., Berti-Dupuis, L., Rivière, M., Spinelli, S., Berna, P., et al. (2002). Crystal structure of the open form of dog gastric lipase in complex with a phosphonate inhibitor. *J. Biol. Chem.*, *277*(3), 2266–2274.

Sandoval, G. (2012). Lipases and phospholipases. *Methods and Protocols. Humana*

Press.
Schaloske, R. H., & Dennis, E. A. (2006). The phospholipase A2 superfamily and its group numbering system. *Biochim. Biophys. Acta*, *1761*(11), 1246–1259.
Scheerer, P., Park, J. H., Hildebrand, P. W., Kim, Y. J., Krauß, N., Choe, H.-W., et al. (2008). Crystal structure of opsin in its G-protein-interacting conformation. *Nature*, *455*(7212), 497–502.
Schindler, P. A., Settineri, C. A., Collet, X., Fielding, C. J., & Burlingame, A. L. (1995). Site-specific detection and structural characterization of the glycosylation of human plasma proteins lecithin:cholesterol acyltransferase and apolipoprotein D using HPLC/electrospray mass spectrometry and sequential glycosidase digestion. *Protein Sci.*, *4*(4), 791–803.
Schneider, B. E., Behrends, J., Hagens, K., Harmel, N., Shayman, J. A., & Schaible, U. E. (2014). Lysosomal phospholipase A2 : A novel player in host immunity to Mycobacterium tuberculosis. *Eur. J. Immunol.*, *00*, 1–11.
Schneider, T. R., & Sheldrick, G. M. (2002). Substructure solution with SHELXD. *Acta Crystallogr. D, 58,* 1772-1779
Schrag, J. D., Li, Y., Cygler, M., Lang, D., Burgdorf, T., Hecht, H. J., et al. (1997). The open conformation of a Pseudomonas lipase. *Structure*, *5*(2), 187–202.
Schwarz, F., & Aebi, M. (2011). Mechanisms and principles of N-linked protein glycosylation. *Curr. Opin. Struc. Biol., 21,* 576- 582
Segrest, J. P., Jones, M. K., De Loof, H., & Dashti, N. (2001). Structure of apolipoprotein B-100 in low density lipoproteins. *J. Lipid Res.*, *42*(9), 1346–1367.
Sensi, C., Simonelli, S., Zanotti, I., Tedeschi, G., Lusardi, G., Franceschini, G., et al. (2014). Distant homology modeling of LCAT and its validation through in silico targeting and in vitro and in vivo assays. *PloS One*, *9*(4), e95044.
Shankaranarayanan, A., Thal, D. M., Tesmer, M. V., Roman, D. L., Neubig, R. R., Kozasa, T., & Tesmer, J. J. (2008). Assembly of High Order G q-Effector Complexes with RGS Proteins. *J. Biol. Chem.*, *283*(50), 34923–34934.
Sigma-Aldrich Co. LLC. (2008, January 8). Endoglycosidases.
Singh, P., Wang, B., Maeda, T., Palczewski, K., & Tesmer, J. J. G. (2008). Structures of rhodopsin kinase in different ligand states reveal key elements involved in G protein-coupled receptor kinase activation. *J. Biol. Chem.*, *283*(20), 14053–14062.
Skretting, G., Blomhoff, J. P., Solheim, J., & Prydz, H. (1992). The genetic defect of the original Norwegian lecithin:cholesterol acyltransferase deficiency families. *FEBS Letters*, *309*(3), 307–310.
Sorci-Thomas, M., Babiak, J., & Rudel, L. L. (1990). Lecithin-cholesterol acyltransferase (LCAT) catalyzes transacylation of intact cholesteryl esters. Evidence for the partial reversal of the forward LCAT reaction. *J. Biol. Chem.*, *265*(5), 2665–2670.
Sorci-Thomas, M., Kearns, M. W., & Lee, J. P. (1993). Apolipoprotein AI domains involved in lecithin-cholesterol acyltransferase activation. Structure: function relationships. *J. Biol. Chem.*, *268*(28), 21403–21409.
Stanley, P. (1989). Chinese hamster ovary cell mutants with multiple glycosylation defects for production of glycoproteins with minimal carbohydrate heterogeneity. *Mol. Cell. Biol., 9(2),* 377-383
Stern, B., Olsen, L. C., & Trösße, C. (2007). Improving mammalian cell factories: The selection of signal peptide has a major impact on recombinant protein synthesis and

secretion in mammalian cells. *Trends Cell Mol. Biol.*

Steyrer, E., Haubenwallner, S., Hörl, G., Gießauf, W., Kostner, G. M., & Zechner, R. (1995). A single G to A nucleotide transition in exon IV of the lecithin: cholesterol acyltransferase (LCAT) gene results in an Arg140 to His substitution and causes LCAT-deficiency. *Hum. Genet.*, *96*(1), 105–109.

Stoffel, R. H., Randall, R. R., Premont, R. T., Lefkowitz, R. J., & Inglese, J. (1994). Palmitoylation of G protein-coupled receptor kinase, GRK6. Lipid modification diversity in the GRK family. *J. Biol. Chem.*, *269*(45), 27791–27794.

Subbaiah, P. V., & Bagdade, J. D. (1978). Demonstration of enzymatic conversion of lysolecithin to lecithin in normal human plasma. *Life Sci.*, *22*(22), 1971–1977.

Subbaiah, P. V., Albers, J. J., Chen, C. H., & Bagdade, J. D. (1980). Low density lipoprotein-activated lysolecithin acylation by human plasma lecithin-cholesterol acyltransferase. Identity of lysolecithin acyltransferase and lecithin-cholesterol acyltransferase. *J. Biol. Chem.*, *255*(19), 9275–9280.

Subbaiah, P. V., Liu, M., & Paltauf, F. (1994). Role of sn-2 acyl group of phosphatidyl choline in determining the positional specificity of lecithin-cholesterol acyltransferase. *Biochemistry*, *33*, 13259–13266.

Szedlacsek, S. E., Wasowicz, E., Hulea, S. A., Nishida, H. I., Kummerow, F. A., & Nishida, T. (1995). Esterification of oxysterols by human plasma lecithin-cholesterol acyltransferase. *J. Biol. Chem.*, *270*(20), 11812–11819.

Taniyama, Y., Shibata, S., Kita, S., Horikoshi, K., Fuse, H., Shirafuji, H., et al. (1999). Cloning and expression of a novel lysophospholipase which structurally resembles lecithin cholesterol acyltransferase. *Biochem. Biophys. Res. Co.*, *257*(1), 50–56.

Terwilliger, T. C., Adams, P. D., Read, R. J., McCoy, A. J., Moriarty, N. W., Grosse-Kunstleve, R. W., et al. (2009). Decision-making in structure solution using Bayesian estimates of map quality: the PHENIX AutoSol wizard. *Acta Crystallogr. D*, *65*(Pt 6), 582–601.

Terwilliger, T. C., Grosse-Kunstleve, R. W., Afonine, P. V., Moriarty, N. W., Zwart, P. H., Hung, L. W., et al. (2008). Iterative model building, structure refinement and density modification with the PHENIX AutoBuild wizard. *Acta Crystallogr. D.*, *64*(Pt 1), 61–69.

Tesmer, J. J. G., Nance, M. R., Singh, P., & Lee, H. (2012). Structure of a monomeric variant of rhodopsin kinase at 2.5 A resolution. *Acta Crystallogr. F, F68, 622-625*

Tesmer, V. M., Kawano, T., Shankaranarayanan, A., Kozasa, T., & Tesmer, J. J. G. (2005). Snapshot of activated G proteins at the membrane: the Galphaq-GRK2-Gbetagamma complex. *Science*, *310*(5754), 1686–1690.

Thiyagarajan, M. M., Stracquatanio, R. P., Pronin, A. N., Evanko, D. S., Benovic, J. L., & Wedegaertner, P. B. (2004). A Predicted Amphipathic Helix Mediates Plasma Membrane Localization of GRK5. *J. Biol. Chem.*, *279*(17), 17989–17995.

Tran, T. M., Jorgensen, R., & Clark, R. B. (2007). Phosphorylation of the beta2-adrenergic receptor in plasma membranes by intrinsic GRK5. *Biochemistry*, *46*(50), 14438–14449.

Trimble, R. B., & Tarentino, A. L. (1991). Identification of distinct endoglycosidase (endo) activities in Flavobacterium meningosepticum: endo F1, endo F2, and endo F3. *J. Biol. Chem.*, *266*(3), 1646–1651.

van Meeteren, L. A., & Moolenaar, W. H. (2007). Regulation and biological activities of

the autotaxin-LPA axis. *Prog. Lipid Res.*, *46*(2), 145–160.
van Pouderoyen, G., Eggert, T., Jaeger, K.-E., & Dijkstra, B. W. (2001). The crystal structure of Bacillus subtili lipase: a minimal α/β hydrolase fold enzyme. *J. Mol. Biol.*, *309*(1), 215–226.
van Tilbeurgh, H., Egloff, M. P., Martinez, C., Rugani, N., Verger, R., & Cambillau, C. (1993). Interfacial activation of the lipase-procolipase complex by mixed micelles revealed by X-ray crystallography. *Nature*, *362*(6423), 814–20.
Vanloo, B., Peelman, F., Deschuymere, K., Taveirne, J., Verhee, A., Gouyette, C., et al. (2000). Relationship between structure and biochemical phenotype of lecithin:cholesterol acyltransferase (LCAT) mutants causing fish-eye disease. *J. Lipid Res.*, *41*(5), 752–761.
Vatter, P., Stoesser, C., Samel, I., Gierschik, P., & Moepps, B. (2005). The variable C-terminal extension of G-protein-coupled receptor kinase 6 constitutes an accessorial autoregulatory domain. *FEBS Journal*, *272*(23), 6039–6051.
Verger, R. (1997). "Interfacial activation"of lipases: facts and artifacts. *Trends in Biotechnology*, *15*(1), 32–38.
Vickaryous, N. K., Teh, E. M., Stewart, B., & Dolphin, P. J. (2003). Deletion of N-terminal amino acids from human lecithin: cholesterol acyltransferase differentially affects enzyme activity toward α-and β-substrate lipoproteins. *Biochim. Biophys. Acta, 1646,* 164-172
Wang, J., Gebre, A. K., Anderson, R. A., & Parks, J. S. (1997). Amino acid residue 149 of lecithin: cholesterol acyltransferase determines phospholipase A2 and transacylase fatty acyl specificity. *J. Biol. Chem., 272(1),* 280-286
Wang, X. L., Osuga, J.-I., Tazoe, F., Okada, K., Nagashima, S., Takahashi, M., et al. (2011). Molecular analysis of a novel LCAT mutation (Gly179 → Arg) found in a patient with complete LCAT deficiency. *J. Atheroscler. Thromb.*, *18*(8), 713–719.
Weber, C. L., Frohlich, J., Wang, J., Hegele, R. A., & Chan-Yan, C. (2007). Stability of lipids on peritoneal dialysis in a patient with familial LCAT deficiency. *Nephrol. Dial. Transpl.*, *22*(7), 2084–2088.
Wiebusch, H., Cullen, P., Owen, J. S., Collins, D., Sharp, P. S., Funke, H., & Assmann, G. (1995). Deficiency of lecithin:cholesterol acyltransferase due to compound heterozygosity of two novel mutations (Gly33Arg and 30 bp ins) in the LCAT gene. *Hum. Mol. Genet.*, *4*(1), 143–145.
Winn, Winn, M. D., Ballard, C.C., Cowtan, K.D., et al. (2011). Overview of the 4 suite and current developments. *Acta Crystallogr. D*, *67*(4), 235–242.
Yang, C. Y., Manoogian, D., Pao, Q., & Lee, F. S. (1987). Lecithin: cholesterol acyltransferase. Functional regions and a structural model of the enzyme. *J. Biol. Chem., 262(7),* 3086-3091
Yang, P., Glukhova, A., Tesmer, J. J. G., & Chen, Z. (2013). Membrane orientation and binding determinants of G protein-coupled receptor kinase 5 as assessed by combined vibrational spectroscopic studies. *PloS One*, *8*(11), e82072.
Yang, X. P., Inazu, A., Honjo, A., Koizumi, I., Kajinami, K., Koizumi, J., et al. (1997). Catalytically inactive lecithin: cholesterol acyltransferase (LCAT) caused by a Gly 30 to Ser mutation in a family with LCAT deficiency. *J. Lipid Res.*, *38*(3), 585–591.
Yap, K. L., Yuan, T., Mal, T. K., Vogel, H. J., & Ikura, M. (2003). Structural Basis for Simultaneous Binding of Two Carboxy-terminal Peptides of Plant Glutamate

Decarboxylase to Calmodulin. *J. Mol. Biol.*, *328*(1), 193–204.
Yi, X. P., Gerdes, A. M., & Li, F. (2002). Myocyte Redistribution of GRK2 and GRK5 in Hypertensive, Heart-Failure-Prone Rats. *Hypertension*, *39*(6), 1058–1063.
Yokoyama, S., Fukushima, D., Kupferberg, J. P., Kézdy, F. J., & Kaiser, E. T. (1980). The mechanism of activation of lecithin:cholesterol acyltransferase by apolipoprotein A-I and an amphiphilic peptide. *J. Biol. Chem.*, *255*(15), 7333–7339.
Zhang, C. L., McKinsey, T. A., Chang, S., Antos, C. L., Hill, J. A., & Olson, E. N. (2002). Class II histone deacetylases act as signal-responsive repressors of cardiac hypertrophy. *Cell*, *110*(4), 479–488.
Zhang, Y. (2008). I-TASSER server for protein 3D structure prediction. *BMC Bioinformatics*, *9*(1), 40.
Zhao, Y., Gebre, A. K., & Parks, J. S. (2004). Amino acids 149 and 294 of human lecithin:cholesterol acyltransferase affect fatty acyl specificity. *J. Lipid Res.*, *45*(12), 2310–2316.
Zhao, Y., Wang, J., Gebre, A. K., Chisholm, J. W., & Parks, J. S. (2003). Negative charge at amino acid 149 is the molecular determinant for substrate specificity of lecithin: cholesterol acyltransferase for phosphatidylcholine containing 20-carbon sn-2 fatty acyl chains. *Biochemistry*, *42*(47), 1013-1025
Zorich, N., Jonas, A., & Pownall, H. J. (1985). Activation of lecithin cholesterol acyltransferase by human apolipoprotein E in discoidal complexes with lipids. *J. Biol. Chem.*, *260*(15), 8831–8837.